ELECTROCHEMICAL AND INFRARED SPECTROSCOPY STUDIES OF AN IONIZABLE SELF-ASSEMBLED MONOLAYER

A Thesis Submitted to

The College of Graduate Studies and Research

In Partial Fulfillment of the Requirements

For the Degree of Master of Science

In the Department of Chemistry

University of Saskatchewan, Saskatoon

By:

SCOTT MICHAEL ROSENDAHL

PERMISSION TO USE

In presenting this thesis in partial fulfillment of the requirements for a Postgraduate Degree from the University of Saskatchewan, I agree that the Libraries of this University may make it freely available for inspection. I further agree that permission for copying of this thesis in any manner, in whole or in part, for scholarly purposes may be granted by the professor or professors who supervised my thesis work or, in their absence, by the Head of the Department or the Dean of the College in which my thesis work was done. It is understood that any copying or publication or use of this thesis or parts thereof for financial gain shall not be allowed without my written permission. It is also understood that due recognition shall be given to me and to the University of Saskatchewan in any scholarly use which may be made of any material in my thesis.

Requests for permission to copy or to make other uses of materials in this thesis in whole or part should be addressed to:

Head of the Department of Chemistry
University of Saskatchewan
Saskatoon, Saskatchewan S7N 5C9
Canada

ABSTRACT

Switchable surfaces, also called ‘smart surfaces’ or ‘controllable surfaces’, respond to changes in their local environment resulting in altered surface properties. There are various environmental perturbations that can cause changes to the surface properties but the focus of this thesis is on the affect of electrostatic potential. Significant evidence is provided from previous reports on electrochemical and infrared spectroscopic experiments suggesting that self-assembled monolayers (SAMs) of 4-mercaptobenzoic acid (4-MBA) undergo protonation-deprotonation by the application of an electric field. However, there are plenty of aspects of this electric field driven protonation-deprotonation mechanisms using carboxylic acid terminated SAMs that are not well understood. Most importantly, there is a lack of model independent measurements to validate this process. As such, experimental techniques utilizing infrared spectroscopy were employed to correlate electrochemical measurements and models.

This body of work demonstrates the importance of the intermolecular hydrogen bonding network on the measured voltammetric peak associated with the protonation-deprotonation of these SAMs. The voltammetric peak height diminishes with increasing exposure to an electrolyte solution. This behaviour is attributed to the replacement of the carboxylic acid protons with electrolyte cations and ultimately the disruption of the hydrogen bonded network.

We attempted to further our *ex-situ* infrared measurements by using an *in-situ* spectroelectrochemical technique. We had some initial successes, presented within, but more work is needed to complete this picture and is beyond the scope of this thesis. To summarize, the protonated state of SAMs of 4-MBA can be driven by the application of an electric field providing a potential platform to build a controllable 'smart surface'.

ACKNOWLEDGEMENTS

I would first like to start off by thanking Dr. Ian J. Burgess for his invaluable support, guidance and patience throughout the time I have spent working with him. I would also like to thank the members of my Advisory Committee and Dr. Robert W.J. Scott for their helpful insight regarding my work. To the members of the Burgess and Scott research groups, thank you for your help and putting up with me.

In addition, this research would not be possible without the financial support of the National Science and Engineering Research Council of Canada (NSERC), and the University of Saskatchewan's Department of Chemistry.

Finally, and most importantly, I owe a special thank you to my family and friends for all the support they have given me throughout the years. Thank you everyone.

TABLE OF CONTENTS

LIST OF FIGURES

LIST OF ABBREVIATIONS

MUA	11-mercaptoundecanoic Acid
4-MBA	4-mercaptobenzoic Acid
AA	Acetic Acid
AFM	Atomic Force Microscopy
ATR	Attenuated Total Reflectance
ATR-FTIR	Attenuated Total Reflectance – Fourier Transform Infrared
CV	Cyclic Voltammogram
cyt-C	cytochrome-C
DAQ	Data Acquisition
DC	Direct Current
EIS	Electrochemical Impedance Spectroscopy
ER-FTIRS	External Reflectance – Fourier Transform Infrared Spectroscopy
FTIR	Fourier Transform Infrared
ILIT	Indirect Laser Induced Temperature-Jump
IR	Infrared
IRRAS	Infrared Reflection-Absorption Spectroscopy
MCT	Mercury Cadmium Telluride
NaPB	Sodium Phosphate Buffer
PAD	Plane of Acid Dissociation
PM-IRRAS	Polarization Modulation – Infrared Reflection-Absorption Spectroscopy

PNIPAam	poly(N-isoproplyacrylamide)
QCM	Quartz Crystal Microbalance
SAM	Self-Assembled Monolayer
SERS	Surface Enhanced Raman Spectroscopy
SNIFTIRS	Subtractively Normalized Interfacial Fourier Transform Infrared Spectroscopy

1. General Introduction to Switchable Surfaces

1.1 Introduction

Switchable surfaces, also called ‘smart surfaces’ or ‘controllable surfaces’, are surfaces that respond to various environmental stimuli by altering their surface properties in relation to modified environmental conditions. Such surfaces are covered by a thin layer of material that when perturbed by an external stimulus can switch between at least two conformational states, each having different properties. Various perturbations can be used to reversibly control switchable surface properties such as photo-illumination [1], electric potential [2, 3] and variations in the surrounding medium [4, 5] (i.e. pH, temperature and pressure). The net result of these external stimuli is a surface whose wettability, conductance and adhesive properties, to name a few, can be strategically altered for various applications in corrosion inhibition [6], self-cleaning materials [7] and ‘biochips’ [8].

A common surface property manipulated with in these systems is surface wettability. A surface is said to be wettable if a drop of solvent, most commonly

water, spreads to become a thin film when placed on the surface. For an ideal switchable surface, application of an external stimulus results in 'de-wetting' whereby the solvent contracts on the surface into a bead with a large contact angle. Applications which could utilize this property are numerous. For example, materials would be capable of self cleaning.

Given the broad scope of this topic, examples of three of the most common types of switchable surfaces are discussed below, namely surfaces based on polymers, metallic oxides and finally using self-assembled monolayers (SAMs).

1.2 Switchable Surfaces based on Polymers and Metallic Oxides

Smart surfaces designed with thin layers of polymers take advantage of 'stimuli-responsive' polymers. Such polymers can undergo dramatic reversible reactions altering their physio-chemical properties in response to external perturbations. These polymer films tend to be very sensitive to modification in the surrounding medium and undergo changes by varying the temperature, light radiation and solvent quality [9].

A commonly studied polymer film utilizing a temperature driven stimulus is poly(N-isoproplyacrylamide), (PNIPAam). PNIPAam undergoes a reversible change in surface wettability as a result of the film becoming hydrated and hydrophilic,

below a critical temperature (the lower critical solution temperature), and becoming dehydrated above that temperature [10]. This change is due to a state transition of the polymer chains going from a disordered random coil structure to a more ordered collapsed structure [9]. It should be noted that this reversible state transition can also occur isothermally by changes in pH [11], ionic strength [12], and electric field [13]. Through the manipulation of any one of these external stimuli, PNIPAam modified surfaces will change from a hydrophilic to a hydrophobic state. One such application could be to control the adhesion of biological cells [14]. Okano *et al.* demonstrated that endothelial cells and hepatocytes can be selectively attached - detached by preparing end-functionalized PNIPAam surface films.

The subject of metallic oxides is primarily dominated by two materials, titanium dioxide (TiO_2) and zinc oxide (ZnO). These two semi-conducting materials have a wide range of technical applications in optics, electronics and acoustics. Both of these thin films, TiO_2 and ZnO, have shown the ability to be reversibly switched between super-hydrophobic and super-hydrophilic surfaces [7]. These two surface states can be toggled by varying the exposure to ultraviolet light, thus modifying the wettability of the surface.

Although surfaces made with polymers and metallic oxides can be made switchable, they have limitations. For example, functionalized polymers of suitable monodispersity are synthetically challenging to produce. Additionally, transduction of signals arising from a switching event is more difficult at insulting (polymer) or

semi-conducting (metal-oxides) surfaces. An excellent alternative to these materials are monolayer films formed on metal surfaces.

1.3 Switchable Surfaces based on Self-Assembled Monolayers

Switchable surfaces based on SAMs have attracted a great deal of research interest. The concept of these systems is to assemble an ordered monolayer of molecules that can be perturbed by various external stimuli, exploiting the state of the SAM. Such perturbations, ranging from light to electrochemical potential, allow for controllable smart surfaces to be designed that find numerous applications in wettability [15] and adhesion [16].

Considering that some SAMs are light perturbed, such as azobenzene (and its derivatives), they undergo reversible photo-isomerization between trans and cis isomers using particular wavelengths of light. When SAMs containing these chemical motifs are exposed to ultraviolet radiation (360nm), such surfaces become more hydrophilic as a result of the polar cis-azobenzene terminus being exposed at the surface. If this same surface is then exposed to blue light (436nm) the resulting cis to trans conformational change of the azobenzene moiety results in the surface becoming more hydrophobic [17]. An interesting application of these surfaces is the controlled mobility of water droplets by applying gradient light intensities of the aforementioned wavelengths near the drop [17]. The result is a change in

isomerization of the azobenzene moiety, due to the light perturbation, producing a surface free energy gradient which drives the motion of the drop on the surface.

Another example of conformational changes of SAMs originates from the application of an electric field to a low-density ioniziable alkanethiolate SAM [18]. When stimulated with an electric field, the ionizable side of the molecule is either drawn to or away from the surface due to the electrostatic effects of the head-group moiety and the surface charge on the metal [18]. The reversible nature of such surfaces allows for controllable adhesive properties of various charged molecules on the surface. However, there are considerable difficulties in creating these surfaces due to the complexity of producing low-density coated gold surfaces.

As an alternative to trying to produce a low-density alkanethiolate SAM while making use of electric fields, an ionizable packed alkanethiol SAM [19] is used instead. In this approach, instead of trying to drive the repulsion – attraction nature of an ionizable head group to the gold substrate, the objective is to modify the SAM terminus' state of ionization. One such example is to force a proton on or off a carboxylic acid terminated alkanethiol. Previous work on these SAMs has demonstrated that through the application of an electric field, such films can have the state of protonation of the carboxylic acid moiety reversibly altered. This modified protonation affects the hydrophobicity [20] and adhesive properties [16] of such films.

The electric field driven protonation-deprotonation mechanism using carboxylic acid terminated self-assembled monolayers is not well understood at present time and as such provides the focus for the current research. Much of the work currently done on this topic has been for long chain alkanoic acid SAMs, for example 11-mercaptoundecanoic acid (MUA). The intensity of the electric-field at the site of the protonation and deprotonation is important in this process. It follows than that the length and motif of the alkanoic linker in the carboxylic acid should influence this reaction. For instance, an aromatic molecule will experience a greater degree of electron delocalization than a long chain alkane molecule and may have profound effects on the electric-field at the COOH terminus. Therefore, we investigated the electric-field driven protonation-deprotonation process for SAMs of a short aromatic molecule, 4-mercaptobenzoic acid (4-MBA), by means of electrochemical and infrared spectroscopic studies.

1.4 References

[1] Nakayama, K.; Jiang, L.; Iyoda, T.; Fujishima, A., *Jpn. J. Appl. Phys. Part 1* **1997**, *36*, 3897.

[2] Prins, M.W.J.; Welters, W.J.J.; Weekamp, J.W., *Science* **2001**, *291*, 277.

[3] Abbott, N.L.; Gorman, C.B.; Whitesides, G.M., *Langmuir* **1995**, *11*, 16.

[4] Crevoisier, D.; Fabre, P.; Corpart, J.; Leibler, L., *Science* **1999**, *285*, 1246.

[5] Minko, S.; Manfred, S., *Polym. Mater. Sci. Eng.* **2000**, *83*, 533.

[6] Mathiyarasu, J.; Pathak, S. S.; Yegnaraman, V., *Corrosion Rev.* **2006**, *24*, 307.

[7] Wang, R.; Hashimoto, K.; Fujishima, A.; Chikuni, M.; Kojima, E.; Kitamura, A.; Shimohigoshi, M.; Watanabe, T., *Nature* **1997**, *388*, 431.

[8] Galaev, I.Y.; Mattiasson, B., *Trends Biotechnol.* **1999**, *17*, 335.

[9] Nath, N.; Chilkoti, A., *Adv. Mater.* **2002**, *14*, 1243.

[10] Sun, T.L.; Wang, G.J.; Lin, F.; Biqian, L.; Yongmei, M.; Lei, J.; Zhu, D.-B., *Angew. Chem. Int. Ed.* **2004**, *43*, 357.

[11] Siegel, R.A.; Firestone, B.A., *Macromolecules* **1988**, *21*, 3254.

[12] Kontturi, K.; Mafe, S.; Manzanares, J.A.; Svarfvar, B.L.; Viinikka, P., *Macromolecules* **1996**, *29*, 5740.

[13] Kwon, I.C.; Bae, Y.H.; Kim, S.W., *Nature* **1991**, *354*, 291.

[14] Takei, Y.G.; Aoki, T.; Sanui, K.; Ogata, N.; Sakurai, Y.; Okano, T., *Macromolecules* **1994**, *27*, 6163.

[15] Abbott, S.; Ralston, J.; Reynolds, G.; Hayes, R., *Langmuir* **1999**, *15*, 8923.

[16] Giz, M.J.; Cheng, G.; Dong, S., *J. Electroanal. Chem.* **1999**, *465*, 72.

[17] Ichimura, K.; Oh, S.-K.; Nakagawa, M., *Science* **2000**, *288*, 1624.

[18] Lahann, J.; Mitragotri, S.; Tran, T.-T.; Kaido, H.; Sundaram, J.; Choi, I.S.; Hoffer, S.; Somorjai, G.A.; Langer, R., *Science* **2003**, *299*, 371.

[19] Burgess, I.; Seivewright, B.; Lennox, R.B., *Langmuir* **2006**, *22*, 4420.

[20] Jordon, C.E.; Frey, B.L., Kornguth, S.; Corn, R.M., *Langmuir* **1994**, *10*, 3642.

2 Carboxylic Acid Terminated Self-Assembled Monolayers as Switchable Surfaces

2.1 Overview of Carboxylic Acid Terminated Self-Assembled Monolayers

A great deal of interest surrounding carboxylic acid terminated self-assembled monolayers (SAMs) stems mainly from the notion of self-assembly, whereby molecules arrange themselves in well organized structures. As such, these systems are useful for the understanding of the solid-liquid interface such as phenomena associated with the stability of colloids, protein adsorption on organic substrates and engineered surfaces where properties such as wettability can be controlled. Another property of these systems is the ease of which they can be prepared and ultimately provide a model interface to study more complicated systems. Nuzzo and Allara were first able to show that a SAM can be prepared by a simple one step adsorption from a dilute thiol solution in ethanol onto a gold substrate [1]. The structure of these SAMs has been extensively studied and it is now well known. Figure 2.1 is an

illustration of a SAM containing 11-mercaptoundecanoic acid (MUA) on a gold substrate.

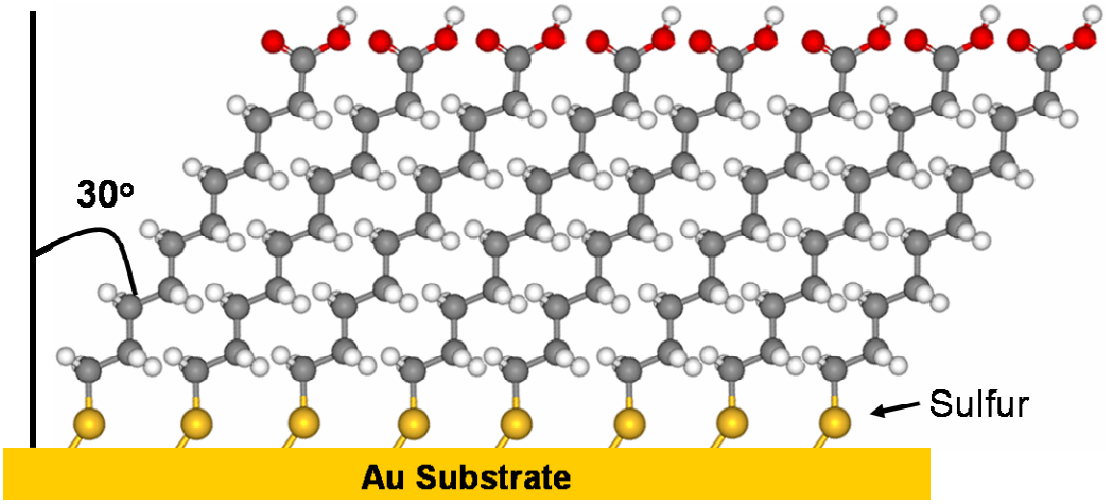

Figure 2.1. Self-assembled monolayer of 11-mercaptoundecanoic acid, MUA, on a gold substrate.

An interesting property of carboxylic acid terminated SAMs is that the carboxylic acid headgroup is ionizable allowing for the surface environment to be modified simply by protonating-deprotonating the acid moiety. There has been a significant amount of research done focusing on how proteins interact with monolayer surfaces. There have also been numerous attempts at utilizing model systems to try and study these complicated interactions. Prime and Whitesides [2] demonstrated early on that SAMs with ω-functionalized alkanethiols on gold surfaces

would make an ideal platform to study such systems and began building SAMs tailored to study protein adsorption. Subsequently, Corn et al. [3, 4] used a variety of experimental techniques to demonstrate that polypeptides (poly-L-lysine) can strongly bind to gold surfaces modified with a deprotonated carboxylic acid terminus (MUA, in the case of their research) and can be further employed to build multi-layered substrates that could be used as adsorption biosensors. This electrostatic layer-by-layer construction of thin films has also been considered by Clark et al [5] in the development of more complicated patterning of surfaces to have regions of specific adsorption.

A particular system that is extensively studied is the adsorption of cytochrome-C (cyt-C) on carboxylic acid terminated SAMs and mixed SAMs of carboxylic acid molecules. Bowden and coworkers have several studies on this topic [6, 7, 8, 9] where they examine the electron transfer processes of electro-active cyt-C adsorbed on acid terminated SAMs. Bowden *et al*. [10] have also looked at the interfacial electron transfer rates of cyt-C on mixed monolayers of COOH-thiols and OH-thiols. From these results they were able to demonstrate dramatic increases in the electron-transfer rates and effectively tune this by altering the composition of the surface.

Besides Bowden and coworkers, other research groups have taken an interest in researching the adsorption of cyt-C onto carboxylic acid terminated SAMs [11, 12]. For instance, Hildebrandt *et al*. [13] also looked at electron transfer kinetics and

Surface Enhanced Raman Spectroscopy (SERS) using silver electrodes. Cytochrome-C has been extensively used in studying protein adsorption onto carboxylic acid terminated SAMs. Other interesting electrochemical adsorption studies have looked at a neural transmitter, dopamine, [14, 15], enzymatic systems [16] and various antibodies [17, 18, 19] for use as biosensors.

Another example of the versatility of carboxylic acid terminated SAMs is the notion of building low-density ioniziable alkanethiolate SAMs [20, 21]. These systems, when manipulated with an electric field cause the ionizable headgroup of the molecule to be drawn to and from the surface due to the electrostatic effects (Figure 2.2).

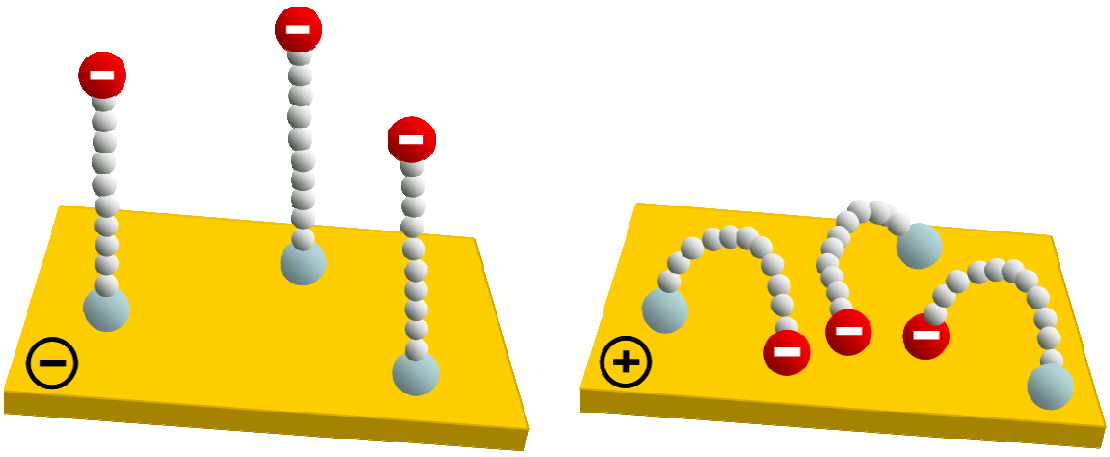

Figure 2.2. Illustration of the conformational transition for Low Density Ionizable SAMs.

This is a reversible process that allows for potential applications where the controllable adhesive properties of the surface can be used to selectively adsorb charged molecules on the surface. However, the major limitation is that low-density ionizable alkanethiolate SAMs are inherently more difficult to prepare. Two examples of low density carboxylic acid terminated SAMs include tuning the hydrophobicity of the interface by the application of an electric potential [20] and by controlling the assembly of two kinds of fluorescently labeled proteins that could go a long way in the design of functional biosensors [21].

These are just some of the applications being used for carboxylic acid terminated SAMs in the literature. The important detail to note is that the ionizable headgroups can be used to create 'smart surfaces' in that the control of these systems is based on perturbations that ionize the head groups. An understanding of what conditions and to what extent carboxylic acid terminated SAMs are ionized is the topic of the next section. This section will discuss how the surface pK_A of an acid SAM shifts significantly from similar acid molecules in the bulk of solution and what impact this has on potential applications. Also, how an electric potential applied to an acid SAM modified electrode can alter the state of protonation of the acid SAM solution interface will be covered. This last statement provides much of the motivation behind the work presented in this thesis as the various aspects of this mechanism are still not well understood.

2.2 Surface pKa related to Carboxylic Acid Terminated Self-Assembled Monolayers

An important aspect of carboxylic acid terminated SAMs is the ability of the headgroup to ionize. That being said, an organic acid SAM can protonate and deprotonate, ionizing the headgroup, following a simple chemical equation.

$$HA_{(SURFACE)} \leftrightarrow H^{+}_{SURFACE} + A^{-}_{SURFACE} \qquad \text{(Equation 2.1)}$$

Associated with this chemical equation is the notion of an equilibrium constant, K_A, as well as a pK_A ($-\log(K_A)$) which is related to the ionization of the acid. This value is essentially a quantitative measurement of the strength of an acid. Lower pK_A values describe stronger acids which indicate large dissociation and vice versa for high values of pK_A. For instance, strong acids such as HCl and $HClO_4$ have very low pK_A values and are considered completely dissociated in water whereas weaker acids such as acetic acid have much higher pK_A values and are only partially dissociated.

What is interesting about SAMs of carboxylic acids is that the pK_A of the surface bound molecules is much higher than that of the free molecule in the bulk solution. Generally, it is much harder to deprotonate, or ionize, carboxylic acid terminated SAMs than their free bulk aqueous molecule counterparts. Several reasons why this could be the case include: ion solvation, hydrogen bonding and interfacial potentials. Knowing this information can provide key insights into

biological processes, including protein folding and adsorption. There has been a great deal of effort to quantify the pK_A for acid SAMs and what causes this difference between bound acid SAM molecules and acid molecules in bulk aqueous environments.

There have been several methods used to try to measure the pK_A value. For instance, measurements have been made using Atomic Force Microscopy (AFM) [22], contact angle titrations [23, 24], Quartz Crystal Microbalance (QCM) titrations [25, 26], indirect laser-induced temperature jump [27] and electrochemical methods [28, 29, 30, 31, 32, 33]. Pooling the results of these various techniques, from different authors, we end up with an interestingly ambiguous literature pK_A value ranging from 5.5 to 9 for the same acid SAM (MUA). In all these studies the transitions from a fully protonated state to a fully deprotonated state are much broader than molecules in bulk solutions but within the literature the range of pH values spanning the transition differs greatly. The explanations of this effect seem equally broad.

Research by Creager and Clarke [23] make a series of contact angle measurements of carboxylic acid SAMs. When a liquid contacts a solid surface, or in our case a SAM covered substrate, the surface of the liquid forms an angle with that surface, termed the contact angle (Figure 2.3). This angle changes as a function of the system, related to effects such as hydrophobicity and electrostatics between the droplet and the surface.

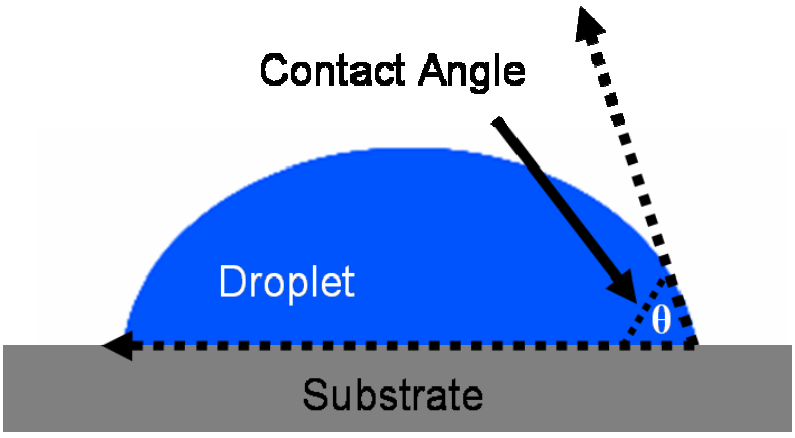

Figure 2.3. Contact angle measured for a droplet of liquid on a solid substrate.

The authors passively incubated their SAMs in ethanolic solutions containing a thiol for 24 hours on to gold coated slides. A passive incubation uses no external driving forces to aid the formation of a SAM. An active incubation typically involves applying an electric potential to the substrate resulting in shorter incubation times but not necessarily more structured SAMs. Following a brief work up, the SAM coated slides were then exposed to the buffered solution of interest, rinsed, and then dried before measuring the contact angle using the same buffered solution. From their results, Creager and Clarke describe at least two different effects for the observed pK_A shifts for their acid SAM molecules, ion solvation energies and interfacial potential effects.

The first contributed effect is due to the ion solvation energetics in the interfacial microenvironment, which indicates the ion solvation energy affects the

position of the acid dissociation equilibrium. In this case, the ion solvation energy is the energy required to break the attraction of the proton associated with the protonated acid SAM to become surrounded by water (solvent) molecules. In conjunction with this is the solvation of the newly formed carboxylate anion. Although, the poor solvation of the proton is the primary effect considered, we also have to consider the solvation energies of the conjugate bases for these acids. If the microenvironment around the acid site was less polar than the solvent, due to a long chain alkanethiol for example, the formation of the charged carboxylate anion would be disfavoured and would shift the pK_A to higher values. There is precedence for this effect stemming from poor solvation of acidic protons in non-aqueous solvents dramatically increasing the pK_A of those organic acids [34].

This leads us to also consider how steric effects around the carboxylate headgroup also increase the pK_A values of surface bound acid molecules. These steric effects arise as the electrostatic interactions with neighbouring molecules change as the acid molecules become dissociated. This change in electrostatics causes a steric hindrance prevent neighbouring molecules from deprotonating. Essentially, the close proximity of the acid moieties, the molecules immobilized on the surface, does not allow for the repulsive interactions to relieve themselves by pushing away from each other. As such, larger forces are required to drive the deprotonation to balance the steric effects resulting in higher pK_A values for acid SAM molecules.

It has been observed that the tensile stress measured for a fatty acid monolayer (on a Langmuir Trough) increases with increasing pH of the aqueous subphase [35]. A possible explanation for this behaviour is the electrostatic repulsion created by neighbouring carboxylate anions after becoming deprotonated. It should also be noted that through the formation of carboxylate anions a loss of intermolecular hydrogen bonding is observed. In the case of the carboxylic acid SAMs, the tensile stress (steric hindrance) created by the deprotonation, can not be relieved through expansion as our molecules are essentially immobilized on the surface. This effectively lowers the acidity of our carboxylic acid SAMs as it becomes harder to deprotonate our molecules shifting the pK_A to higher values.

Bain and Whitesides [24] have also looked at contact angle measurements in an attempt to explain the shift in pK_A. The authors created mixed SAMs in an attempt to control the surface composition. By effectively controlling the ratio of $HS(CH_2)_{10}CH_3$ and $HS(CH)_{10}CO_2H$ molecules in their incubating solutions, the authors created mixed monolayer systems by co-adsorption of the thiols with some control of composition [36]. From their results, they also attributed the shift in pK_A of surface bound acid molecules to the free energy of ionization. Using a similar procedure to that of Creager and Clarke [23], samples were extensively cleaned and immersed in the desired pH buffer, dried and then contact angle measurements made using the same buffer. Bain *et al*. conclude that the contact angles start to decrease with increasing pH, suggesting that as the interface is becoming more polarized and essentially deprotonated.

The second observed effect by Creager and Clarke is due to an interfacial potential [23]. This effect has been used quite frequently to describe the shift in pK_A values for acid SAMs at charged interfaces and is the topic of much discussion. An interesting situation arises when monolayers of acids are ionized, effectively deprotonated, in that the interfacial potential difference is created by the acid SAMs themselves. Smith and White [33], Fawcett and Fedurco [37] and Burgess *et al*. [38] have considered this phenomenon extensively and this is the subject of the next section of this chapter. Briefly, however, Smith and White [33] have noted that an apparent pK_A shift (on the order of: $\Psi F/2.303RT$, where Ψ is the interfacial potential, F is Faraday's constant with R and T have their usual meanings being the gas constant and temperature) is to be expected for molecules in SAMs opposed to those found in the bulk of solution. It is important to note that the interfacial potential distribution does depend in part on the dielectric properties of the interface.

Another surface technique used to study the surface acid-base properties of carboxylic acid terminated SAMs is Atomic Force Microscopy (AFM). AFM essentially consists of a microscopic cantilever with an atomically sharp tip (often called a probe) that is used to scan a surface [39]. As the probe scans the surface, forces between the tip and the surface cause the cantilever to deflect according to Hooke's Law. This deflection is measured by irradiating a laser spot on the top surface of the cantilever and measuring the changes in reflection as the probe interacts with the surface. If the properties of the surface are changing, for example

the ionization of an acid-SAM due to proton dissociation, the results will alter the force measured between the tip and the surface.

Hu and Bard [22] made use of AFM to measure the double-layer forces between a silica probe and a carboxylic acid terminated SAM in aqueous solutions. Their results conclude that the interaction between the probe and the SAM covered substrate is strongly related to the solution pH. Through a series of calculations and by applying a theoretical model of the interface, Hu and Bard were able to correlate the surface potential to the solution pH resulting in a titration curve. Extracting the pK_A from this curve, the authors report a value of 7.7 for 3-mercaptopropionic acid compared to that of the solution phase acid of 4.3 [40]. They attribute this shift in pK_A of 3.4 units to the electrostatic interactions present at the monolayer-electrolyte interface as the acid-SAMs become deprotonated.

Quartz Crystal Microbalance (QCM) techniques have also been used to try and determine the surface pK_A of acid-SAMs. Briefly, QCM is a technique that essentially measures a mass over an area by measuring a change in the frequency of a quartz crystal resonator [41]. If there is a change of mass associated with material coming on or off of the crystal the resonance also changes. Specifically, in this case however, QCM measures the change in the hydrodynamic properties near the crystal, effectively structural changes in the electrolyte in contact with the SAM moiety, which subsequently undergo measurable changes when protonated acid-SAMs become deprotonated and vice-versa.

Sugihara *et al*. [25] and Wang *et al*. [26] used the method of QCM to illicit the surface pK_A of acid-SAM systems. They stressed that molecules immobilized on a surface will have different properties than those in the bulk phase. They attribute this difference to the different local environments surrounding the molecules in a SAM versus those in the bulk of solution. The major contributing factor is the electrostatic interactions of the acid moieties being in close proximity to each other in the SAM. The authors suggest that this allows for strong lateral attractive and repulsive electrostatic interactions between SAM molecules which are not observed for molecules in the bulk phase. This influences the dissociation of the surface acid molecules forcing the pK_A to higher values than those found in the bulk.

Similarly, Wang *et al*. [26] describes this result and suggests that this observed behaviour is similar to that of the phase transition reported for fatty-acid monolayers on aqueous subphases. The measured pK_A values for acid SAMs, with much broader transitions, can be attributed to hydrogen bonding stabilizations with a protonated SAMs and nearest-neighbour electrostatic interactions stemming from the deprotonated carboxylate anion.

Looking at fatty acid monolayers on aqueous subphases, Wang *et al*. note that the behaviour they are seeing in their QCM measurements can be partially explained by the film undergoing an expansion upon the increase in the pH of the aqueous subphase. They suggest that as the acid SAM becomes deprotonated, there is an increase in the electrostatic repulsion between neighbouring carboxylate anions

(consistent with Sugihara *et al*. [25]) but introduce the notion about a loss of hydrogen bonding between the acid groups. Due to the acid-SAMs being immobilized on the surface, they are not able to relieve this stress. As such, these two effects work in combination with each other to decrease the acidity (raising the pK_A) of the acid SAM compared to molecules in the bulk as the system wants to minimize these effects.

Smalley *et al*. [27] used the method of Indirect Laser-Induced Temperature-Jump (ILIT) to determine the acidity, surface pK_A, of monolayers composed of MUA. The technique involves measuring the rapid change (<10 ns) in the open-circuit potential of the SAM and electrolyte interface effected by a small laser-induced temperature perturbation (2-5°C). This technique is able to measure the pK_A of an acid SAM because the magnitude of the ILIT response is proportional to the potential gradient at the interface which is a function of the degree of ionization of the SAM. The authors' results report a surface pK_A of 5.7 at electrolyte ionic strengths of 0.10M and the pK_A at 4.4 with 1.0M ionic strength electrolytes.

Several groups have performed electrochemical titrations [28, 29, 30, 31, 32, 33] to try and determine the surface pK_A of acid SAMs and relate the apparent shift back to electrostatic interactions. Molinero *et al*. [28] examined the effects of attaching Ferrocene, from the electrolyte, to acid monolayers. Cheng *et al*. [29] used $Fe(CN)_6^{3-}$ and $Ru(NH_3)_6^{3+}$ redox probes to measure dissociation of the carboxylic acid headgroup in direct contact with the solution. Zhao *et al*. [30] did similar

experiments using cyclic voltammograms of acid SAMs in phosphate buffered solutions containing $Fe(CN)_6^{3-}$ probe. All three groups were able to use the resulting measured Faradaic current, essentially the electron transfer, of the probe to investigate the degree of dissociation of the acid headgroup. This is due to the simple electrostatic arguments where a negatively charged ion will be repelled by a negatively charged surface, in this case the deprotonated acid SAM, resulting in no Faradaic current being measured.

Kim *et al*. [31] performed an electrochemical impedance titration to study the in-place electrostatic forces that affect the surface pK_A of acid SAMs. An interesting result of their research is that the ionic strength of the electrolyte is not significant to the shift at strengths greater than 0.1M. Accordingly, the authors discuss that the major attributing factor to the shift in the surface pK_A is related to hydrogen bond formation between the acids headgroups and the local dielectric properties around them. By looking at two different acid SAMs, in pure as well as several mixed monolayers, the authors reveal that the surface pK_A is sensitive to the number of possible intermolecular interactions, such as hydrogen bonding and electrostatic repulsive interactions.

Another interesting study using electrochemical techniques to probe the surface pK_A of acid SAMs was done by Kakichi *et al*. [32] where they collected double-layer capacitance measurements at various electrolyte pHs. The authors describe their technique to be an extremely sensitive measure of the protonated-

deprotonated state of the monolayer which successfully determines the associated surface pK_A. They also note that their titration curves are much broader than titrations of similar molecules measured in the bulk of solution. They attribute this broadening, as well as a shift of 4 pH units compared to bulk molecules, to the electrostatic repulsion between the deprotonated headgroups of the acid SAMs. The authors also suggest the importance of the state of the microscopic environment around the acid headgroups in the SAMs in determining the titration characteristics. A similar method was also reported by Bryant and Crooks [42] to determine the surface pKA of 4-mercaptopyridine and 4-aminothiophenol. Under a very similar formulation Smith and White [33] postulated a voltammetric approach to studying the surface acid-base equilibrium, and ultimately surface pK_A, of acid-SAMs.

An interesting aspect of carboxylic acid terminated SAMs is that the apparent pK_A of the acid molecules in the SAM is shifted to higher numbers than the same molecule in the bulk of solution. There have been numerous attempts to report a surface pK_A for MUA SAMs using several techniques resulting in large discrepancies. Several factors are proposed (i.e. ion solvation, steric hindrance, interfacial potentials, hydrogen-bonding and local solvent structure) for the cause of this shift in pK_A and they have been discussed. Of interest, is the application of an electric field to carboxylic acid terminated SAMs to drive the protonation-deprotonation reaction. This is the topic of the next section and ultimately is the underlying theme of this thesis.

2.3 Thermodynamic Model of Electric-Field Driven Protonation - Deprotonation

A specific thermodynamic model developed by Smith and White [33] was used to describe the effect of the interfacial potential on acid-SAMs. Specifically, we will look at how this model can explain the electric-field driven protonation – deprotonation process of acid SAMs. From previous sections within this chapter, various factors and theories behind the apparent shift in pK_A of carboxylic acid SAMs have been described. In no particular order, the pK_A of a surface-confined molecule is affected by the polarity of the surface, the microenvironment around the acidic surface sites and interfacial electrostatic fields.

Focusing on interfacial electrostatic fields, consider a system with an irreversibly adsorbed carboxylic acid terminated monolayer on an electrified surface in a 1:1 electrolyte solution. An assumption of this model is that all the acid - base moieties of the acid headgroups lie in a plane, referred to as the plane of acid dissociation (PAD), which is a distance, *d*, from the metal surface (Figure 2.4).

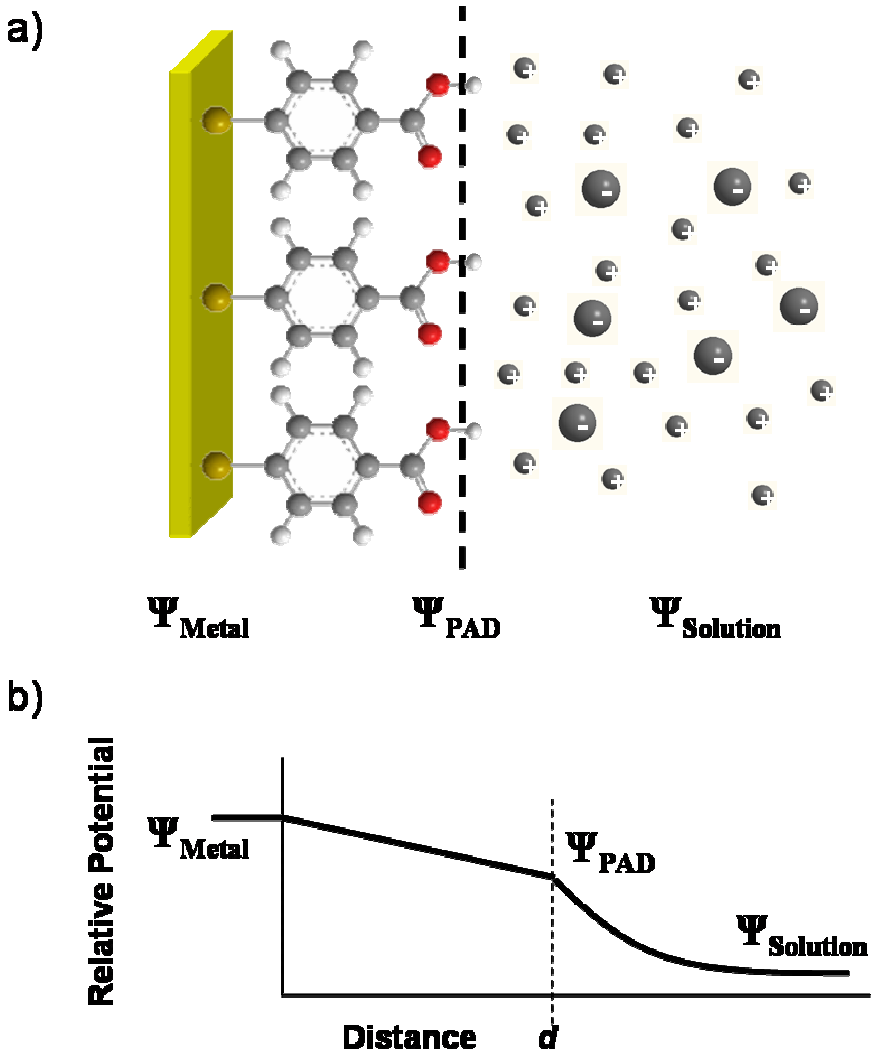

Figure 2.4. (a) Representation and (b) electrostatic potential distribution of an adsorbed 4-MBA SAM on a metal surface in an electrolyte solution.

A dielectric region exists between the metal surface and the PAD where the potential across this region is described by a linear profile (Parallel Plate Capacitor/Helmholtz Model). As illustrated in Figure 2.4(b), beyond the PAD, the potential drops

exponentially as the distance increases from the surface in accordance to Gouy-Chapman theory for the diffuse part of the electrical double-layer. Fawcett *et al*. [37, 43] extended Smith and White's model to include a Stern layer adjacent to the monolayer (this perturbs the potential profile shown in Figure 2.4(b)). However, as the thermodynamic consequences of the model are independent of the exact nature of the double layer this simpler profile will suffice for this discussion.

Considering the above model by modifying the degree of dissociation of the acid headgroups the electric-field within the monolayer also changes. Thinking about this concept in reverse, by applying an appropriate electric-field to the SAM, it is expected that a dissociation of the acid headgroups will occur. That is, the surface acid-base equilibrium will shift in response to the potential applied to the metal surface in an attempt to minimize the free energy at the interface. In theory this is a potential controlled surface that could be used as a 'smart surface'.

The equilibrium for the reaction (Equation 2.1) occurring at the surface described above can be re-written in terms of an equilibrium constant with the fraction of the surface that is dissociated, denoted as θ.

$$K_A = \frac{\theta}{1-\theta}\left[H^+_{(SURFACE)}\right] \qquad \text{(Equation 2.2)}$$

An important concept to consider in the above equation (Equation 2.2) is how to properly define the proton concentration, $\left[H^+_{(SURFACE)}\right]$, in the volume element just

beyond the PAD. The surface proton concentration requires a definition of a surface volume. One possible speculation is that the distribution of protons in the area from the PAD to the bulk of solution follows a Boltzmann distribution (Equation 2.3). Dissociated protons at the PAD can populate distances extending into the bulk region up to a maximum distance, *x*, which would be determined by their thermal energy, kT (where k is the Boltzmann's Constant). Thus the surface volume is simply the product of the surface area and the thermal diffusion distance, *x*. To get around this problem, the proton concentration $\left[H^{+}_{(SURFACE)}\right]$ is rewritten in terms of a macroscopic property, the bulk proton concentration $\left[H^{+}_{\infty}\right]$, through the Boltzmann distribution [22, 44] as follows:

$$\left[H^{+}_{(SURFACE)}\right] = \left[H^{+}_{\infty}\right] \exp\left(\frac{-F\psi}{RT}\right) \qquad \text{(Equation 2.3)}$$

where F is Faraday's constant, ψ is the electrostatic potential at the PAD, R is the gas constant and T is the temperature. The negative log of Equations 2.2 and 2.3 (resulting in Equations 2.4 and 2.5), can be combined and re-written yielding the final result reached by Smith and White [33]. This relationship (Equation 2.6) can now be used to relate the fraction of the acid SAM that is deprotonated to the solution pH and the electrostatic potential at the PAD.

$$pK_A = pH_{(SURFACE)} - \log\frac{\theta}{1-\theta} \qquad \text{(Equation 2.4)}$$

$$pH_{(SURFACE)} = pH_{\infty} + \frac{F\psi}{2.303RT} \qquad \text{(Equation 2.5)}$$

$$\log\frac{\theta}{1-\theta} = pH_{\infty} - pK_{A} + \frac{F\psi}{2.303RT} \qquad \text{(Equation 2.6)}$$

It is interesting to note that by ignoring the electrostatic contribution (third term on the right side of Equation 2.6), the expected result for the acid-base equilibrium for the acid molecules is found.

Another characteristic of the model proposed by Smith and White [33, 45] is that it describes the total differential capacity, C_T, of the interface by looking at the contributions from the aliphatic backbone of the film (modeled as a Helmholtz Capacitor), C_F, the degree of ionized acid-headgroups, C_θ, and the diffuse part of the electric double layer, C_S.

$$\frac{1}{C_T} = \frac{1}{C_F} + \frac{1}{C_S + C_\theta} \qquad \text{(Equation 2.7)}$$

The contribution of the ionized acid-headgroups, $C_{\theta,}$ a pseudo-capacitance, in Equation 2.7 is expressed as the follows (Equation 2.8) [33, 45, 46]:

$$C_\theta = \left(\theta^2 \Gamma_{TOTAL} / RT\right)\theta(1-\theta) \qquad \text{(Equation 2.8)}$$

where Γ_{TOTAL} is the total concentration of both acidic and basic forms of acid SAM present on the surface and R,T and θ are defined as above. Also, Equation 2.7 shows that at pH values far from the pK_A the film is fully protonated or deprotonated at all

potentials and thus Equation 2.7 simplifies to contributions of the film, C_F, and the diffuse layer, C_S only. However, in electrolyte solutions where the pH is near the pK_A, Equation 2.7 reveals that the degree of dissociation of the acid SAM can be affected by the electrode's potential. This alters C_θ and now there is a contribution to the total differential capacity of the interface.

In the absence of any redox-chemistry the capacitive current for an electrode where the potential is swept at a constant rate, ν, is given by the following expression [45]:

$$i = \nu A C_T \qquad \text{(Equation 2.9)}$$

where A is the area of the electrode and *i* is the resulting measured current. Given the definition for C_T (Equation 2.7), as the potential is swept on an acid SAM modified electrode at a pH near the surface pKA it is expected that the degree of ionization of the acid headgroups changes (Equation 2.6) as per the above discussion. This ultimately affects the value of C_θ resulting in a measurable change in the current producing a voltammetric peak. The expected maximum height of this peak is associated with the situation where $\theta = 0.5$ [33, 45, 38].

The model presented here by Smith and White [33] shows the electrostatic potential at the PAD-solution interface plays an important role in the degree of protonation-deprotonation of the acid SAM. By working in electrolyte solutions where the pH is near the surface pK_A for an acid SAM modified electrode, the degree

of ionization of the acid headgroups may be controlled. From electrochemical experiments it is expected that there will be a measured voltammetric peak associated with this process resulting in an electric-field driven protonation-deprotonation reaction.

2.3.1 Kinetics of the Model

One particular aspect of the model presented by Smith and White [33] is that their model predicts the height of the voltammetric peak associated with the electric-field driven protonation-deprotonation of acid SAM modified electrodes will be the same at all pH values. Experimentally, however, the measured voltammetric peak height changes as a function of electrolyte pH suggesting a maximum peak height when the pH is equal to the pK_A of the surface bound acid. This curious result led to the work done by Burgess *et al*. [38], where they studied the kinetic effects of electric-field driven protonation-deprotonation which may explain this experimental evidence.

To that end, Burgess *et al*. [38] carried out a series of electrochemical measurements, including Electrochemical Impedance Spectroscopic (EIS) and Cyclic Voltammetry, of MUA SAMs on polycrystalline gold electrodes. Their experimental results allowed for an analytical expression to be derived describing the impedance of the protonation-deprotonation reaction for MUA SAMs. This description includes contributions to the total current due to the kinetics from changes in the degree of

dissociation of the acid headgroup. This model successfully described the observed pH dependence on the voltammetric peak height associated with the MUA SAM protonation-deprotonation reaction.

The authors [38], however, point out that although their model accurately predicts the experimentally observed behaviour, the forward and backward rate constants for the protonation-deprotonation reactions are required for verification. Although, Burgess *et al*. [38] have outlined a methodology using EIS and FTIR spectroscopy to experimentally acquire the rate constants, there is still a need to provide model independent measurements to validate the protonation – deprotonation of acid terminated SAMs.

2.4 Conclusion

Carboxylic acid terminated self-assembled monolayers are a very interesting system to study in that the acid terminus is capable of undergoing reversible protonation – deprotonation reactions under the appropriate conditions. By controlling these conditions, one can foresee how such systems can result in 'smart surfaces'. Given this potential, there have been numerous studies looking at adsorption of various biological molecules to these SAMs and their use for biological molecule detection. To this end, there has been significant research done in an attempt to explain the various system properties.

An interesting aspect of carboxylic acid terminated SAMs is that the apparent pK_A of the acid molecules in the SAM is shifted to higher numbers than the same molecule in the bulk of solution. This suggests that it is much harder to deprotonate acid SAM molecules on a surface than in the bulk of solution. There have been numerous attempts [22, 23, 24, 25, 26, 27, 28, 29, 30, 31, 32, 33] to try and determine how much the pK_A shifts as well as the cause of this shift. Several factors have been proposed (i.e. ion solvation, steric hindrance, interfacial potentials, hydrogen-bonding and local solvent structure) to try and explain this effect, but considering how convoluted each effect can be, it is very difficult to provide an exact cause to this shift in pK_A for acid SAMs.

In this chapter, we considered in detail, a model proposed by Smith and White [33] which neatly shows a change in the pK_A of acid SAMs as a result of an interfacial electrostatic potential. From this model we described a thermodynamic equation (Equation 2.7) that links the degree of proton dissociation to the potential applied to the metal substrate. This model shows that a voltammetric peak should be measurable, by performing electrochemical experiments on acid SAM modified electrodes, for the protonation-deprotonation process.

Experimentally, however, the measured voltammetric peak height changes as a function of electrolyte pH which is not accounted for in the original model of Smith and White [33]. Burgess *et al*. [38] attempted an explanation by linking the kinetics involved in the protonation – deprotonation reactions and accurately explained this

phenomenon. Ultimately, a situation has been described where the surface acid-base equilibrium shifts in response to the potential applied at the metal surface. In theory, this sets the fundamental understanding for a system where a potential controlled surface has been created that could be used in applications requiring 'smart surface'.

Given the potential of carboxylic acid terminated SAMs to be used as 'smart surfaces' our research efforts to further the understanding of these systems is an effort to provide a possible platform for future applications. A description of our research, results and conclusions will be elaborated upon in the following chapters. Briefly, we will look at the electric-field driven protonation-deprotonation process of SAMs consisting of 4-mercaptobenzoic acid (4-MBA), a carboxylic acid aromatic thiol, using a combination of electrochemistry and surface sensitive infrared spectroscopic techniques. The reason to study SAMs of 4-MBA stems from the vast majority of research focusing on long alkanoic acid molecules for the electric-field protonation-deprotonation reaction. 4-MBA being a short, aromatic molecule is different in structure and thus exhibits different electrochemical properties compared to long chain alkane acid SAMs. For example, the PAD of 4-MBA SAMs is closer to the electrode than MUA SAMs. In addition, the aromatic nature of the benzene group results in electron delocalization which perturbs the dielectric properties of the SAM. For these reasons studying shorter, aromatic SAM systems extends the Smith and White model beyond the prototypical examples.

2.5 References

[1] Nuzzo, R.G.; Allara, D.L., *J. Am. Chem. Soc.* **1983**, *105*, 4481.

[2] Prime, K.L.; Whitesides, G.M., *Science* **1991**, *252*, 1164.

[3] Jordon, C.E.; Frey, B.L.; Kornguth, S.; Corn, R.M., *Langmuir* **1994**, *10*, 3642.

[4] Frey, B.L.; Jordan, C.E.; Kornguth, S.; Corn, R.M., *Anal. Chem.* **1995**, *67*, 4452.

[5] Clark, S.L.; Hammond, P.T., *Langmuir* **2000**, *16*, 10206.

[6] Tarlov, M.J.; Bowden, E.F., *J. Am. Chem. Soc.* **1991**, *113*, 1847.

[7] Clark, R.A.; Bowden, E.F., *Langmuir* **1997**, *13*, 559.

[8] Kasmi, A.E; Wallace, J.M.; Bowden, E.F.; Binet, S.M.; Lindermann, R.J., *J. Am. Chem. Soc.* **1998**, *120*, 225.

[9] Song, S.; Clark, R.A.; Bowden, E.F.; Tarlov, M.J., *J. Phys. Chem.* **1993**, *97*, 6564.

[10] Kasmi, A.E; Wallace, J.M.; Bowden, E.F.; Binet, S.M.; Lindermann, R.J., *J. Am. Chem. Soc.* **1998**, *120*, 225.

[11] Arnold, S.; Feng, Z.Q.; Kakiuchi, T.; Knoll, W.; Niki, K., *J. Electroanal. Chem.* **1997**, *438*, 91.

[12] Li, J.; Cheng, G.; Dong, S., *J. Electroanal. Chem.* **1996**, *416*, 97.

[13] Hildebrandt, P. Murgida, D.H., *Bioelectrochemistry* **2002**, *55*, 139.

[14] Malem, F.; Mandler, D., *Anal. Chem.* **1993**, *65*, 37.

[15] Giz, M.J.; Duong, B.; Tao, N.J., *J. Electroanal. Chem.* **1999**, *465*, 72.

[16] Barrias, C.C.; Martins, M.C.L.; Miranda, M.C.S.; Barbosa, M.A., *Biomaterials* **2005**, *26*, 2695.

[17] Frederix, F.; Bonroy, K.; Laureyn, W.; Reekmans, G.; Campitelli, A.; Dehaen, W.; Maes, G., *Langmuir* **2003**, *19*, 4351.

[18] Wang, H.; Castner, D.G.; Ratner, B.D.; Jiang, S., *Langmuir* **2004**, *20*, 1877.

[19] Kepley, L.J.; Crooks, R.M.; Ricco, A., *Anal. Chem.* **1992**, *64*, 3191.

[20] Lahann, J.; Mitragotri, S.; Tran, T.-N.; Kaido, H.; Sundaram, J.; Choi, I.S.; Hoffer, S.; Somorjai, G.A.; Langer, R., *Science* **2003**, *299*, 371.

[21] Liu, Y.; Mu, L.; Liu, B.H.; Zhang, S.; Yang, P.Y., Kong, J.L., *Chem. Commun.* **2004**, 1194.

[22] Hu, K.; Bard, A., *Langmuir* **1997**, *13*, 5114.

[23] Creager, S.E.; Clarke, J., *Langmuir* **1994**, *10*, 3675.

[24] Bain, C.D.; Whitesides, G.M., *Langmuir* **1989**, *5*, 1370.

[25] Sugihara, K.; Shimazu, K.; Uosaki, K., *Langmuir* **2000**, *16*, 7101.

[26] Wang, J.; Frostman, L.M.; Ward, M.D., *J. Phys. Chem.* **1992**, *96*, 5224.

[27] Smalley, J.F.; Chalfant, K.; Feldber, S.W.; Nahir, T.M.; Bowden, E.F., *J. Phys. Chem. B* **1999**, *103*, 1676.

[28] Molinero, V.; Calvo, E.J., *J. Electroanal. Chem.* **1998**, *445*, 17.

[29] Cheng, Q.; Brajter-Toth, A., *Anal. Chem.* **1992**, *64*, 1998.

[30] Zhao, J.; Luo, L.; Yang, X.; Wang, E.; Dong, S., *Electroanalysis* **1999**, **11**, 1108.

[31] Kim, K.; Kwak, J., *J. Electroanal. Chem.* **2001**, *512*, 83.

[32] Kakichi, T.; Iida, M.; Imanayashi, S.-I.; Niki, K., *Langmuir* **2000**, *16*, 5397.

[33] Smith, C.P; White, H.S., *Langmuir* **1993**, *9*, 1.

[34] Izutsh, K., *Acid-Base Dissociation Constants in Dipolar Aprotic Solvents*; Blackwell, London, 1990.

[35] Wang, J.; Frostman, L.M.; Ward, M.D., *J. Phys. Chem.* **1992**, *96*, 5224.

[36] Bain, C.D.; Evall, J.; Whitesides, G.M., *J. Am. Chem. Soc.* **1989**, *111*, 7155.

[37] Fawcett, W.R.; Fedurco, M.; Kovacova, Z., *Langmuir* **1994**, *10*, 2403.

[38] Burgess, I.; Seivewright, B.; Lennox, R.B., *Langmuir* **2006**, *22*, 4420.

[39] Bard, A.J.; Faulkner, L.R., *Electrochemical Methods Fundamentals and Applications, 2nd Edition*, Copyright 2001 John Wiley & Sons, Inc., New York, New York, pp. 666.

[40] Forlano, P.; Olabe, J.A.; Magallanes, J.F.; Blesa, M.A., *Can. J. Chem.* **1997**, *75*, 9.

[41] Bard, A.J.; Faulkner, L.R., *Electrochemical Methods Fundamentals and Applications, 2nd Edition*, Copyright 2001 John Wiley & Sons, Inc., New York, New York, pp. 725.

[42] Bryant, M.A.; Crooks, R.M., *Langmuir* **1993**, *9*, 385.

[43] Andreu, R.; Fawcett, W.R. *J. Phys. Chem.* **1994**, *98*, 12753.

[44] Caspers, J.; Goormaghtigh, E.; Ferreira, J.; Brasseur, R.; Vandenbranden, M.; Ruysschaert, J.-M., *J. Colloid Interface Sci.* **1983**, *91*, 546.

[45] White, H.S.; Peterson, J.D.; Cui, Q.; Stevenson, K.J., *J. Phys. Chem. B* **1998**, *102*, 2930.

[46] Creager, S.E.; Wooster, T.T., *Anal. Chem.* **1998**, *70*, 4257.

3 Analysis of 4-Mercaptobenzoic Acid Self-Assembled Monolayers by Cyclic Voltammetry and Fourier Transform Infrared External Reflectance Spectroscopy

3.1 Introduction

There have been several studies on long chain carboxylic acids on conductive metals surfaces showing protonation-deprotonation of the terminal acid moiety by adjusting the pH of the surrounding medium as well as by applying an appropriate electric field [1, 2, 3, 4]. These results were the basis for choosing 4-mercaptobenzoic acid (4-MBA) SAMs to examine the electric-field driven process. Our primary motivation was to extend the results from long alkane chain carboxylic acid molecules to a smaller carboxylic acid molecule with a benzene backbone. In the process we will also investigate the molecular structure of such systems by means of External Reflectance Fourier Transform Infrared Spectroscopy (ER-FTIRS).

The fundamental theoretical model we are following is that of Smith and White [1] where they describe the electric-field driven protonation-deprotonation control of a carboxylic acid terminated molecule bound to a metal surface. We wish to extend this model beyond Smith and White [1], and the subsequent work done by Burgess *et al.* [2] and Fawcett *et al*. [4], to include details about how intermolecular hydrogen bonding and electrolyte ion-exchange affect this process.

3.2 Experimental

Materials and Reagents

4-Mercaptobenzoic acid (90%), KOH (Semiconductor Grade, 99%), NaF (99.99%), NaOH (ACS Grade), $NaClO_4 \cdot H_2O$ (>99%), $KClO_4$ (>99%), $Ca(ClO_4)_2 \cdot 4H_2O$ (>99%), Na_2HPO_4 (ACS Grade), NaH_2PO_4 (ACS Grade) and $HClO_4$ (Ultrahigh Purity Grade) were all purchased from Sigma Aldrich and were used as received. Ethanol (95%) was purchased from Commercial Alcohols Inc. (Brampton ON, CA). Ultrapure acetic acid (Environmental Grade Plus, 99.6%) was obtained from Alfa Aesar. All aqueous solutions were formed from Milli-Q (>18.2 MΩ cm^{-1}) water. The procedure for fabricating the polycrystalline bead electrodes from gold wire (Alfa Aesar, 99.99%) consisted of melting the gold wire with a propane torch until a bead was formed. The gold bead was then immersed in aqua regia (3:1 HCl/HNO_3) to remove any surface impurities and then re-melted. This procedure was repeated several times until the molten gold displayed no visible contaminates.

Following this, the gold bead electrode was electrochemically polished in 50 mM $KClO_4$ by cycling the potential into the surface oxidation/oxide stripping peaks. Gold-coated silicon wafers (Platypus Technologies, LLC, Madison, WI, USA) were used for the IR measurements.

Self-Assembled Monolayer Preparation

The polycrystalline gold bead working electrodes were initially cleaned by immersion in Piranha solution (3:1 H_2SO_4:H_2O_2) for a minimum of 30 min, followed by copious rinsing with Milli-Q (>18.2 MΩ cm^{-1}) water. These electrodes were then flame annealed and quenched with Milli-Q (>18.2 MΩ cm^{-1}) water. The procedure for the gold-coated silicon slides consisted of sonication for 2 min in ethanol to degrease the surface. This method for preparing the gold-coated silicon wafers was preferred as attempts to use UV/Plasma treatments resulted in poor quality SAM formations. Following the above mentioned cleaning procedures, the gold substrates (bead electrodes and/or gold-coated silicon wafers) were immersed in 1 mM 4-MBA ethanolic solutions for 24 hours. We found that shorter time passive incubations resulted in 4-MBA SAMs that did not exhibit any protonation-deprotonation voltammetry. Instead, the electrochemistry resulted in the charging envelope seen for non-functionalized alkane SAMs. A plausible explanation is that for shorter incubation times we do not create as tightly a packed film compared to those SAMs formed in long time incubations. This could result in weaker intermolecular

hydrogen bonding within the SAM. Therefore, to be consistent we only analyzed 4-MBA SAMs prepared after a long term incubation of 24 hours.

To finish off the preparation of the SAMs, the substrates were soaked in Milli-Q (>18.2 MΩ cm^{-1}) water for 10 min before being dried under a blanket of Argon for 3 hours before taking measurements. We found that by drying the SAM coated substrates in Argon for 3 hours helped to anneal the SAM on the surface and resulted in much better electrochemistry showing the protonation-deprotonation voltammetric peak.

3.2.1 Cyclic Voltammetry

Electrochemical experiments were conducted using the electrochemical technique of cyclic voltammetry. In cyclic voltammetry the working electrode potential, in a three electrode configuration, is ramped linearly as a function of time (known as the scan rate) as shown in Figure 3.1(a). The potential is measured between the working and the reference electrodes while the current is measured between the working and the counter electrodes. These measurements are typically made using a Potentiostat (an instrument used to control the potential applied to the working electrode) and a data collection system. The collected data is then plotted as current (*i*) versus potential (E) resulting in a cyclic voltamogram (CV) (Figure 3.1(b)) [5].

From such a plot, detailed information about Faradic (electron passing from the metal surface to a molecule, or vice versa) and non-Faradic processes (capacitive charging) can be examined relativity easily. To gather more information from a CV one has to apply a theoretical model for the interface. In the absence of a redox-active molecule the electrode/electrolyte interface can be modeled as a resistor and capacitor in series (Figure 3.1(c)). Fitting the experimental data to this simple model we can make broad statements about the state of the system and changes in the surface structure.

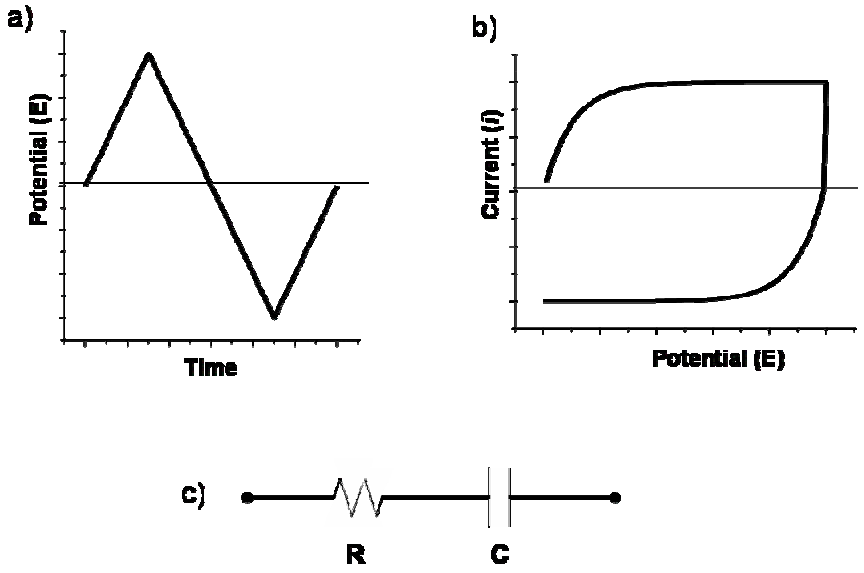

Figure 3.1. Cyclic voltammetric perturbation (a) and the resulting voltammogram (b) for the basic case of a resistor and capacitor in series (c).

In our research, the electrochemical measurements (three-electrode arrangement) used to analyze the electric field driven protonation - deprotonation of 4-MBA SAMs were performed in an all-glass sealed cell, which was connected to the

external reference electrode (Ag/AgCl, saturated KCl) via a salt bridge. The counter electrode was a loop of gold wire which was flame annealed before every experiment. All the glassware used for an experiment was heated in a mixture of H_2SO_4 and HNO_3 (2:1 by volume) and then rinsed copiously and soaked overnight in Milli-Q (>18.2 MΩ cm^{-1}) water prior to every experiment. All electrolytes used were de-oxygenated with Argon before the introduction of the working electrode and a continual blanket of Argon was maintained above the electrolyte during all electrochemical experiments. Measurements of the cyclic voltammetry signals were done using a computer controlled system, consisting of a HEKA Potentiostat PG590 (HEKA, Mahone Bay, NS, Canada). Data was collected using a multifunction DAQ card (PCI 6251 M Series, National Instruments Corporation, Austin, TX, USA) and *in-house* software written in the LabVIEW (National Instruments Corporation, Austin, TX, USA) environment.

3.2.2 Fourier Transform Infrared External Reflectance Spectroscopy

Infrared (IR) spectroscopy deals with the interaction of infrared radiation with matter, usually resulting in the vibrational and rotational motions of molecular bonds. Classically, the infrared portion of the electromagnetic spectrum is subdivided into three distinct research regions; namely the near-, mid- and far- infrared regions (Figure 3.2). Briefly, the near-infrared region (14000-4000 cm^{-1}) of the spectrum is that closest to the visible portion of the electromagnetic spectrum and thus shorter

wavelengths and higher energies. The far-infrared region (400-10 cm^{-1}), that lying closest to the microwave region, is suited to study lower energy pure rotational properties [6]. Finally, the area of the electromagnetic spectrum we are interested in for this research is the mid-infrared region (4000-400 cm^{-1}). Whereas the far-infrared region is excellent for rotational spectroscopy and the near-infrared region does become complicated as the excited harmonic vibrations become convoluted on top of lower energy electronic transitions; the mid-infrared region of the spectrum provides us with the best region to study fundamental vibrational (and coupled rotational-vibrational) modes.

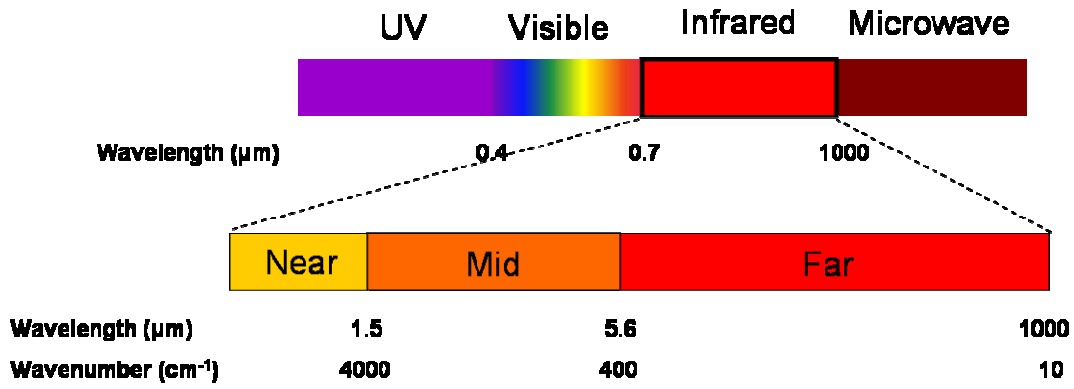

Figure 3.2. Infrared Region of the Electromagnetic Spectrum

In order to study the interactions of IR radiation on matter, several topics must be discussed. Following the brief discussion on how the measurements are physically made, there will be details discussing the theory behind these measurements.

Currently, most mid-infrared spectroscopic measurements are made using a Fourier Transform Infrared (FTIR) spectrometer. In typical absorption spectroscopy, the amount of energy absorbed as the incident radiation is passed through or reflected off a sample then goes through a dispersive element before being measured at a detector. In FTIR spectroscopy, the main difference is that the incident radiation, which comes from a continuum source, is passed through an interferometer (usually Michelson type) first before passing through or reflecting off of a sample. The Michelson interferometer consists of two mirrors (one fixed, the other moveable) and a beam splitter (for mid-IR usually made out of KBr) arranged as shown in Figure 3.3 [7, 8].

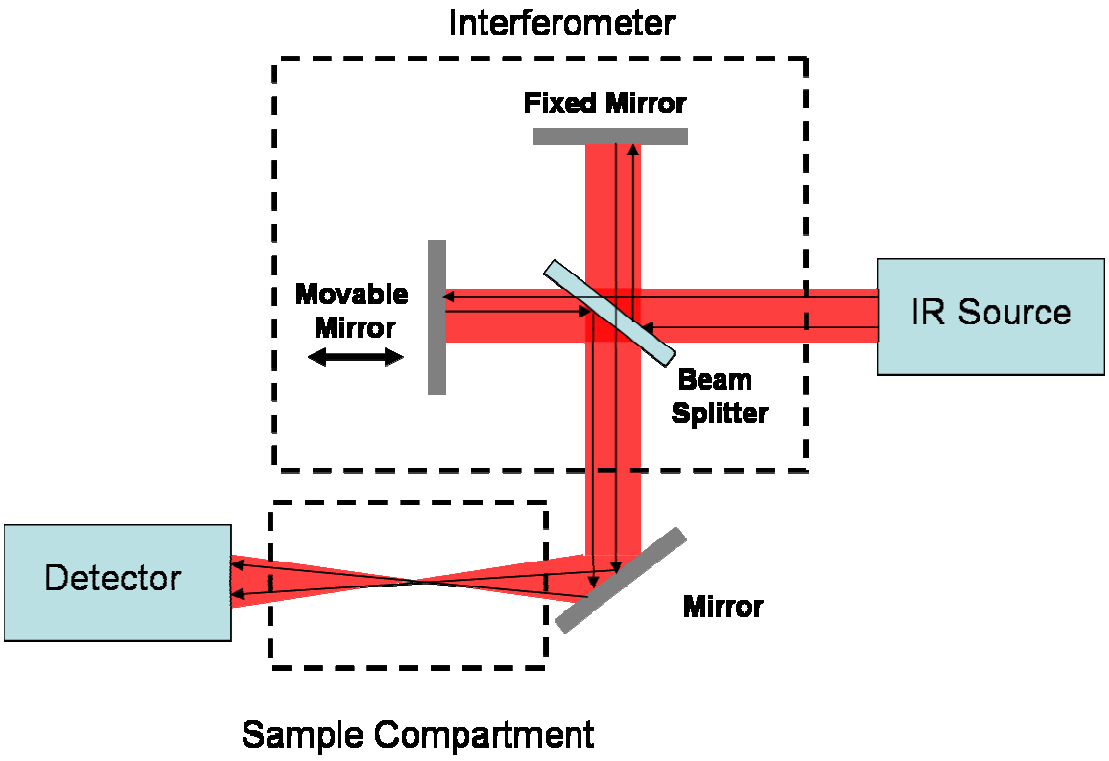

Figure 3.3. Single-beam FTIR Spectrometer using a Michelson interferometer.

The IR radiation travels through the beam splitter to the fixed mirror and then back through the beam splitter before interaction with the sample and measured by the detector. In the other arm of the interferometer, the IR radiation travels through the beam splitter and reflects off the moveable mirror back to the beam splitter before passing through the sample and subsequently measured by the detector. By moving the moveable mirror, we fundamentally change the pathlength of one of the beams. This results in the two beams falling in and out of phase with each other at various wavelengths [7, 8]. The detector measures these signals as the superposition, co-addition of the two beams, resulting in a signal that is effectively related to the spectrum. The spectrum is then mathematically obtained by using a Fourier Transform operator on the collected interferogram data shifting the data from the time domain into the frequency domain. The main advantage to using a FTIR spectrometer over a conventional dispersive spectrometer is that a single spectrum can be measured faster, because essentially all the infrared frequencies are sampled simultaneously, and this allows for multiple samples to be collected and averaged in a shorter amount of time improving the sensitivity (signal to noise ratio) [7].

To discuss the physical aspects of a molecular vibration, molecular vibrations of a diatomic molecule will be examined. As a first approximation molecular vibrations are described by a harmonic oscillator model [9]. This simple model describes a mass connected to a massless spring whereby the mass is under the action of the restoring force, proportional to the spring constant (k), associated with the

spring. With this model, the potential energy is proportional to the square of the displacement and ultimately we can arrive at the frequency of this vibration, ν, by (Equation 3.1):

$$\nu = \left(\frac{k}{m}\right)^{1/2} (2\pi)^{-1} \qquad \text{Equation (3.1)}$$

where k is the spring constant and m is the mass [9]. We can extend this model now to describe molecular vibrations by considering the spring to be the bond between two atoms. This bond will have an associated spring constant, based on the strength of the bond between the atoms and by associated vibronic coupling; and ultimately a resonant frequency at which this bond will vibrate [9]. As such, if the appropriate energy is supplied to the system, by the light source of the spectrometer, the atoms connected by a bond will oscillate at a particular fundamental frequency. By measuring where this frequency occurs, we can deduce information about the bond type [9].

By adding more atoms to a molecule, the possibility of more vibrationic motions, also called modes, are introduced. A general starting position when considering the number of fundamental modes possible with a molecule is to consider the number of degrees of vibrational freedom. If a molecule is non-linear, it is expected to have 3N-6 degrees of freedom, where N is the number of atoms, and for linear molecules, 3N-5 degrees of freedom [10]. For example, if we were to consider water, which is a nonlinear molecule, we would expect to have three fundamental

modes of vibration. We may, however, not be able to measure all of these vibrations and this is the topic of the following section.

The vibrational spectrum of a molecule can be further complicated when we consider that vibrations can be coupled. This potentially leads to more infrared absorptions then those calculated by looking at the number of degrees of freedom for a molecule. For example, given a methylene group and a benzene ring Figure 3.4 represents some of the possible vibrational modes [10].

3.2.2.1 Infrared Selection Rules

Although the number of expected vibrations can be calculated from the number of degrees of freedom of a given molecule, usually fewer numbers of absorptions are measured. There are many factors that contribute to this discrepancy to the number calculated degrees of freedom. For instance, there are several instrumentation limitations such as absorptions with low intensities that can not be resolved instrumentally, or absorptions that are outside the spectral range of detection within the instrument, or those modes that are IR – inactive.

Generally speaking, a vibrational transition is said to be infrared active if the dipole moment, μ, of the molecule changes during the vibration [9]. This statement defines our selection rules and applies for all molecules that are randomly oriented in

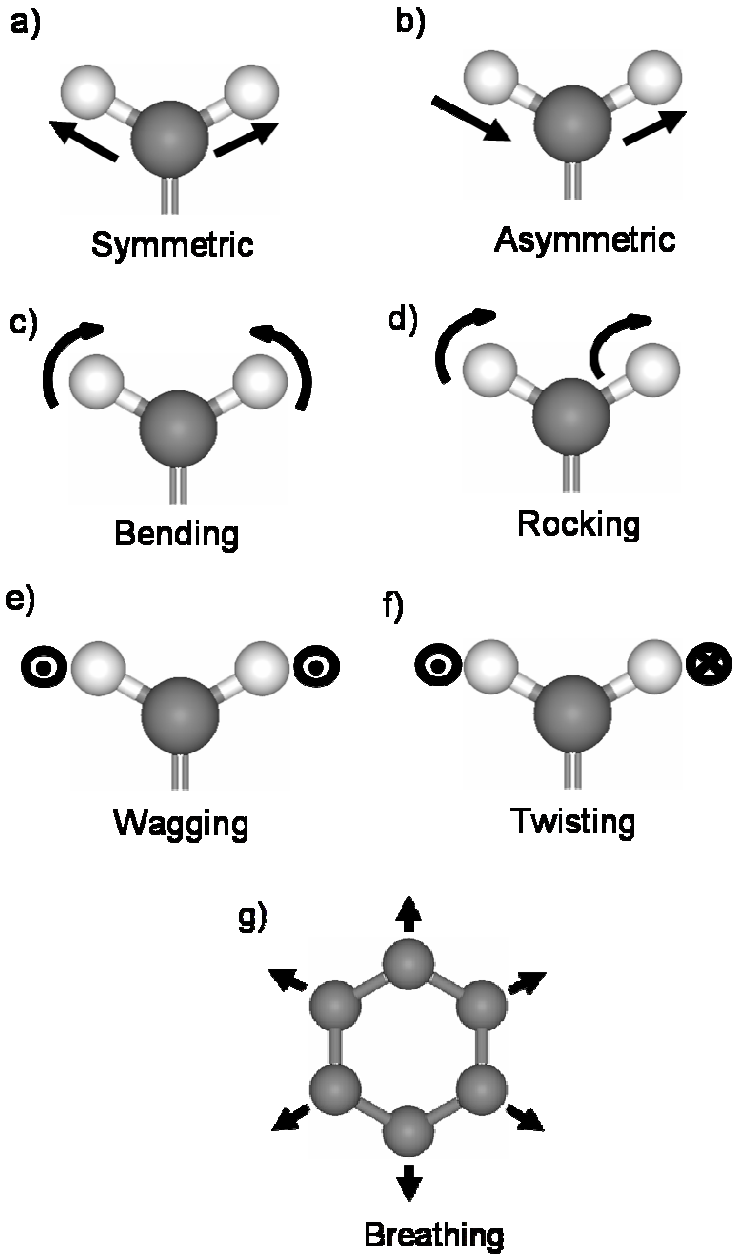

Figure 3.4. The six vibrational modes available for the atoms in a methylene group and the breathing vibration for a ring compound: symmetrical (a), anti-symmetrical (b) stretches, scissoring (c), rocking (d), wagging (e), twisting (f) and the benzene ring breathing mode (g).

the sample medium. Below is an example of an allowed and forbidden infrared vibration transitions (Figure 3.5).

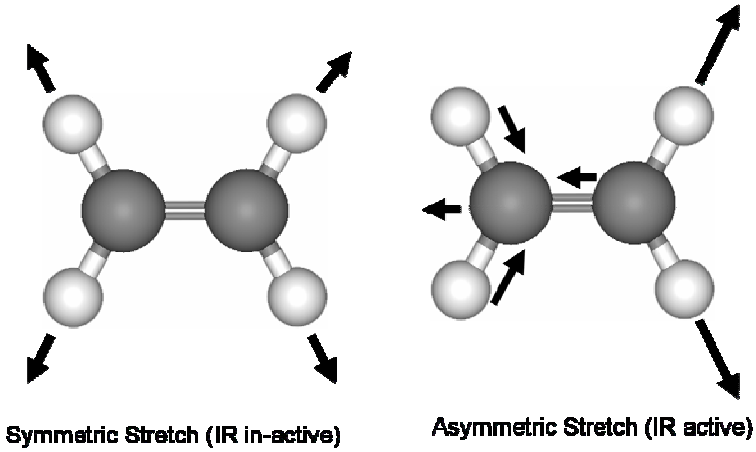

Figure 3.5. Selected example of infrared active and in-active vibrational motions.

The selection rules indicate which transitions might be observed in the spectrum. A real spectrum contains different band intensities varying from very strong to very weak. The selection rules do not distinguish differences in intensity rather they merely indicate which transitions are expected to have zero intensity (based on the harmonic oscillator approximation briefly discussed earlier) and which will have non-zero intensities [9]. Those transitions predicted to have zero intensity are said to be forbidden but the selection rules and those predicted to be non-zero are said to be allowed. Transitions predicted to be allowed in the infrared are said to be infrared active and are dependent on the symmetry of the molecule [9].

3.2.2.2 Surface Selection Rules

Now consider a molecule bound to a surface where an IR reflectance technique is being employed. A few new selection rules for these vibrational transitions need to be introduced. First consider the IR beam incident on the surface (before and after reflection) and secondly the orientation of the proposed vibrational transition. The IR radiation has two limiting polarization states of its electric-field vector, one parallel to the surface of reflection (s-polarized) and the other perpendicular to the surface (p-polarized). After the IR beam is reflected off of the surface, the s-polarized component of the radiation undergoes a 180^{o} phase shift resulting in a complete cancellation of its electric-field vector (Figure 3.6(a)) [11]. The p-polarized component does not undergo this same phase shift and after the reflection the vector sum of incident and reflected electric fields leads to an enhancement in its intensity (Figure 3.6(b)) [11]. Given this enhancement for p-polarized light, molecules having components of their vibrational dipole moments in the same direction as the p-polarized IR light (perpendicular to the surface) will be enhanced.

This observation defines our *surface selection rules*; in that only those vibrations that result in a net change of the dipole moment, μ, of the transition and whose transition dipole moment has a component perpendicular to the surface will have non-zero intensities [11].

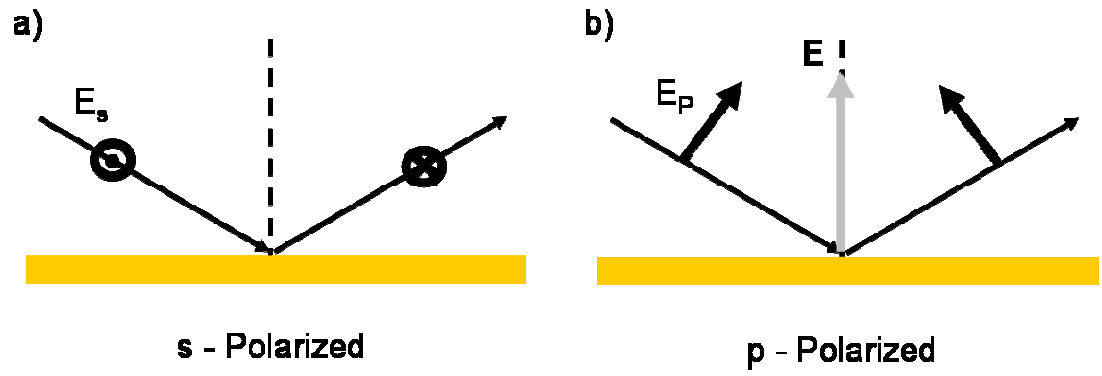

Figure 3.6. Electric-field vectors before and after reflection for (a) s-polarized and (b) p-polarized infrared radiation. In the case of p-polarized radiation, demonstrating the resulting electric-field enhancement.

In the research presented here, FTIR spectroscopy and the surface selection rules previously presented are utilized. Particularly, the technique of External Reflectance FTIR Spectroscopy (ER-FTIRS) will be used. In this technique a measured change in the incident and reflected IR beam due to various absorptions of molecules on the surface is done. These changes are measured using a FTIR spectrometer.

The external reflectance infrared spectroscopic measurements were made using a Pike Technologies External Reflection Spectroscopy (ERS) Accessory (VeeMax II. Pike Technologies, Madison, WI, USA) in the sample compartment of a Nicolet 6700 Fourier Transform Infrared (FTIR) Spectrometer (ThermoFisher Scientific, Madison, WI, USA) (Figure 3.7).

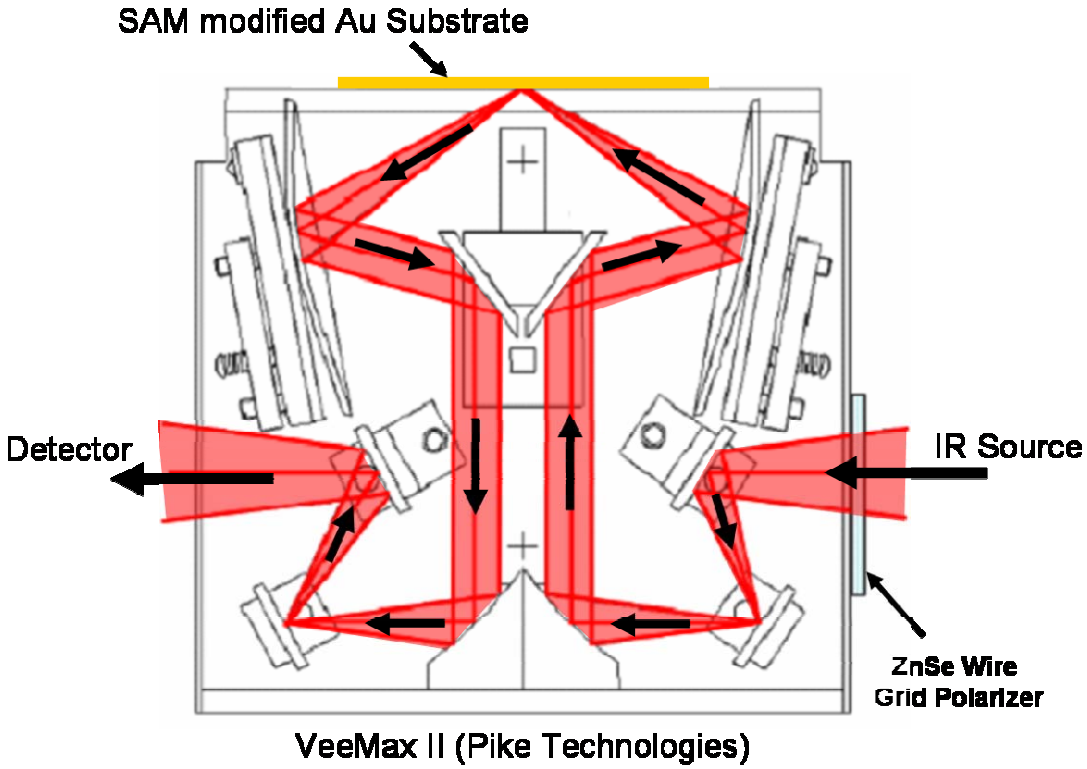

Figure 3.7. Experimental setup for External Reflectance Fourier Transform Infrared Spectroscopy (ER-FTIRS) using a VeeMax II Reflectance Accessory (Pike Technologies).

The incidence infrared light was p-polarized using a wire-grid polarizer and measured at a grazing angle (70^{o}) normal to the gold-coated silicon wafers. By working at a grazing angle of incidence and using p-polarized radiation reflecting off a metal surface, we produce an electric field at the surface that is able to interact strongly with molecules bound perpendicular to the surface [11]. This results in an enhancement of IR absorptions at the surface and is referred to as a surface enhancement technique allowing the measurement of monolayers. The FTIR Spectrometer and ERS Accessory were both purged with dried CO_2-scrubbed air

supplied by a purge gas generator (Parker Balston FT-IR Purge Gas Generator 75-62, Parker Hannifin Corporation, Haverhill, MA, USA) to eliminate potential signal interferences. Each spectrum was recorded using signal averaging of 1000 scans at a resolution of 2 cm^{-1}. The reflectance (absorbance), R, was then calculated from $-\log_{10}(R/R_0)$ where R_0 was the IR spectrum of a bare gold slide.

3.3 Results

3.3.1 Electrochemical Results

A typical family of 4-MBA SAM CVs is plotted in Figure 3.8 using a 50 mM NaF electrolyte. There is a distinct pair of peaks, centered at an apparent formal potential of -200 mV versus Ag/AgCl, present in these voltammograms.

Based on the work presented by Arihara *et al*. [12], and by our own experiments, these peaks are not related to the reductive desorption (and subsequent re-adsorption) which occurs significantly more negative of -500 mV vs $Ag/AgCl_{(SAT)}$, of 4-MBA on polycrystalline gold. Another fact about the observed voltammetric peaks is that they are not the result of a Faradaic process but instead have been attributed to the electric-field driven protonation-deprotonation of the COOH moiety [1, 2, 3, 4].

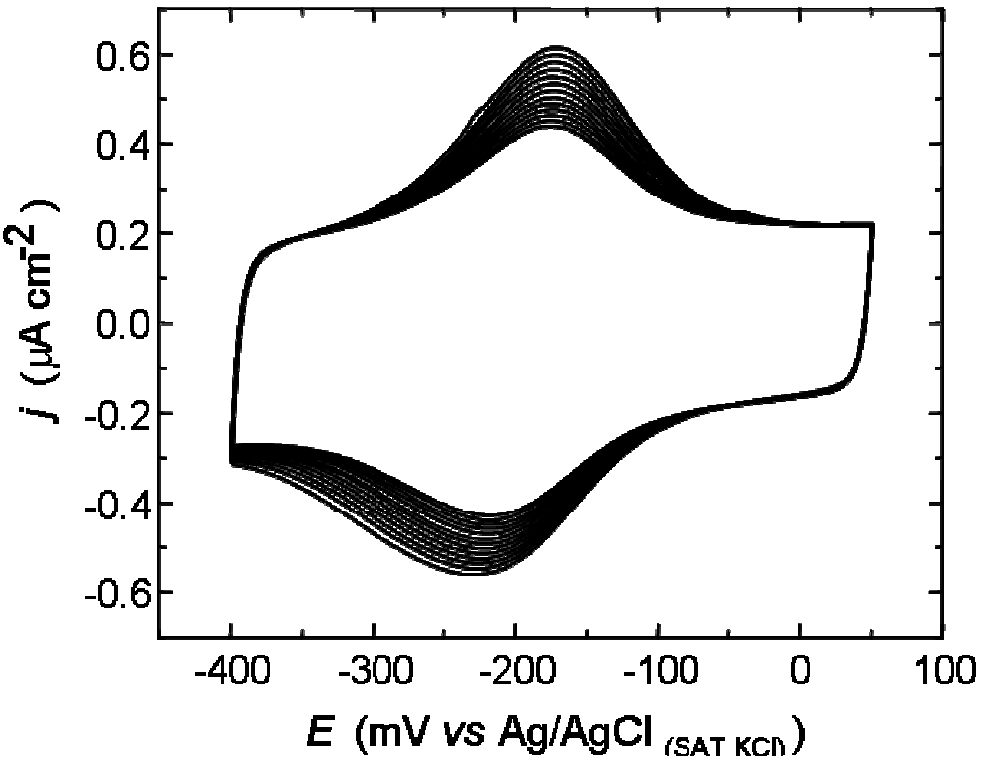

Figure 3.8. Typical family of CVs for 4-MBA SAMs under continued potential cycling in 50 mM NaF electrolyte solution adjusting the pH to 8.3 using NaOH.

Similar CVs have been reported for 11-mercaptoundecanoic acid (MUA) SAMs on various metal electrodes in various electrolytes [2, 3, 13, 14] with some noticeable differences. Firstly, the regions of our CVs well removed from the peak, have roughly twice the magnitude for measured current values than those reported for MUA. This difference can be explained by the large aliphatic tail in MUA compared to the benzene backbone of 4-MBA. Using a Helmholtz description of the interface, the decrease in the inner layer capacity associated with MUA can be rationalized by the increased distance between the electrode surface and the charged carboxylic acid

head group. The second, and probably most striking difference, is the drop in peak current with increasing scan number. This effect has not previously been reported in electrochemical studies of MUA SAMs. As such, we investigated this phenomenon further with several experiments where we applied a DC potential (on either side of the voltammetric peaks) or held our system at the open-circuit potential for an equivalent 'scanning' period of time and still measured this attenuation.

This peak current attenuation will be expanded upon later, but our hypothesis is that an exchange of COOH protons with the cationic ions from the electrolyte solution occurs. As this exchange takes place, the applied electric field is unable to drive the cation off (as it could with the proton due to differences in binding strengths) the carboxylate moiety shutting down the protonation-deprotonation process. As a preliminary experiment, to test this hypothesis, we measured the anodic peak height as a function of scan number for varying electrolyte concentrations (50 mM and 1 mM NaF) and plotted the results in Figure 3.9. From Figure 3.9, it is apparent that an increased concentration of cations in solution results in faster attenuation of the voltammetric peak. More experiments were preformed to test our hypothesis.

The model proposed by Smith and White [1], discussed in detail in the previous chapter, successfully predicts that the peak position should shift as a function of the pH of the surrounding electrolyte. This aspect of the model was examined for its applicability towards SAMs formed by 4-MBA. In order to test this

model and to ensure adequate control of the pH we used 5 mM ionic strength sodium phosphate buffer (NaPB) electrolytes. This provided a satisfactory compromise between buffering capacity and concentration of cations in solution (~10 mM Na^+ at the pH values studied). At this concentration level, we were able to repetitively cycle the potential long enough to obtain the information required (peak potentials) before the peak heights decayed to the background level. We were reluctant to use lower concentrations of the buffer due to possibly diminishing the buffering capacities of such solutions. We compared voltammograms (Figure 3.10) at the same pH (8.5) between 50 mM NaF and 5 mM total ionic strength NaPB electrolytes and found the results to be similar within experimental error.

Figure 3.11 is the resulting plot of the anodic peak potentials as a function of the electrolyte's (NaPB) pH. Each point in the plot was determined by measuring the CVs of freshly prepared electrolytes at different pHs with newly prepared 4-MBA SAM covered electrodes. The rationale behind preparing a new 4-MBA SAM for each pH electrolyte was to eliminate any potential false measurements as a result of extended cycling of the SAM covered electrodes. We can see from the plot that by fitting a linear function to the data points that we have slope of -70 mV/decade as the pH is increased.

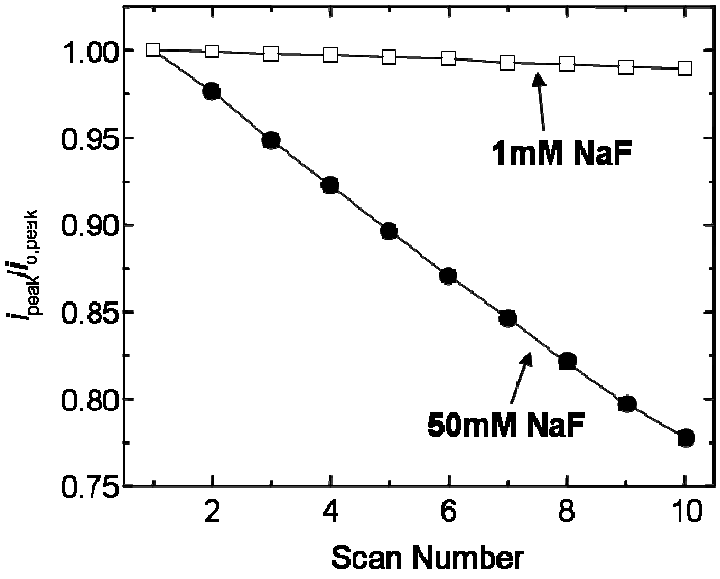

Figure 3.9. Voltammetric peak attenuation of 4-MBA SAMs on polycrystalline gold electrodes in 1 mM and 50 mM NaF electrolytes. The values of the anodic voltammetric peak are normalized to the initial scan peak height.

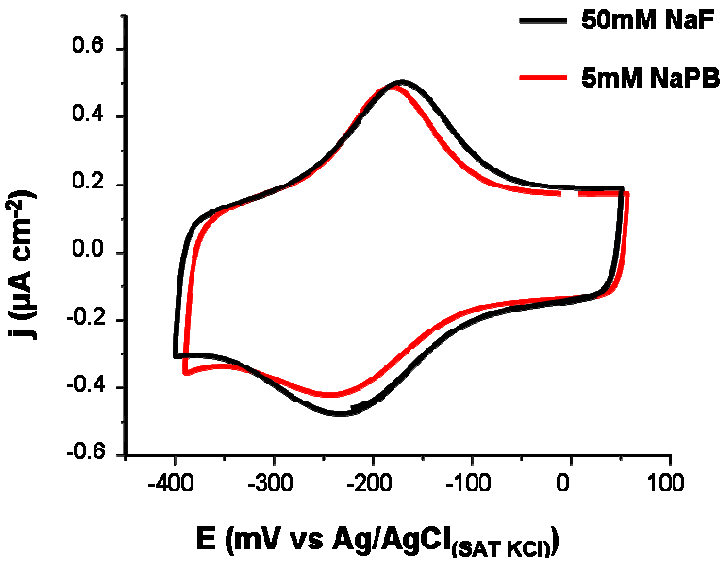

Figure 3.10. Comparison of CVs for 4-MBA SAMs on polycrystalline gold electrodes between 50 mM NaF and 5 mM total ionic strength NaPB electrolytes at the same pH (8.5).

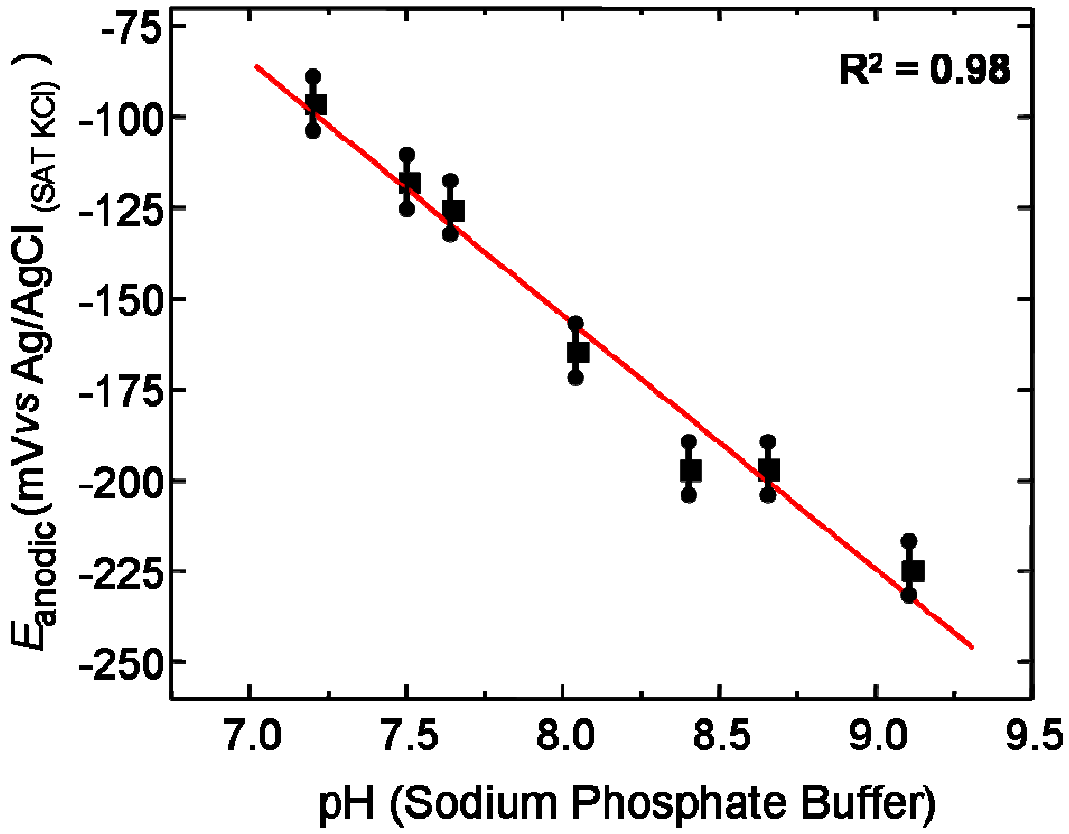

Figure 3.11. pH dependency on anodic peak potential for 4-MBA SAMs on polycrystalline gold electrodes. pH control was accurately achieved by using sodium phosphate buffers.

This is in close agreement with previous results reported by Burgess *et al*. for MUA SAMs on polycrystalline gold for the electric-field driven protonation-deprotonation process [2]. From previous work on MUA SAMs it was also observed that the height of the voltammetric peak was also dependent on pH [2, 3]. This observation is in contrast to the theory described by Smith and White [1] who

suggested that there is no dependence pH dependence on peak height. However, no statements to this effect using our SAMs of 4-MBA could be made as there was a rapid decrease in the peak height as a function of scan number. This fact made it very difficult to provide a quantitative description of the pH dependence on peak height.

3.3.2 Fourier Transform Infrared External Reflectance Spectroscopic Characterization

Unfortunately, given only the electrochemical results the chemical structure of the 4-MBA films can only be inferred by previous studies and models for similar SAMs. Due to the sensitive nature of the chemical structure of the 4-MBA film, External Reflectance - Fourier Transform Infrared Spectroscopy (ER-FTIRS) was used for further characterization. This technique has been previously utilized by Wells *et al.* [15] for 4-MBA monolayers adsorbed on gold surfaces revealing detailed information on the state of the carboxylic acid headgroup. A significant feature of ER-FTIRS spectra of protonated acid SAMs are the carbonyl stretches in the 1750-1690 cm^{-1} region. The infrared features present in this region can be further subdivided into three distinct carbonyl groups (Figure 3.12) consisting of: monomeric (non-hydrogen bonded) (~1735 cm^{-1}), carbonyl groups that form in-plane, single-hydrogen bonded acyclic dimers (~1720 cm^{-1}) and finally head-to-head dimers (~1700 cm^{-1}) [16, 17, 18].

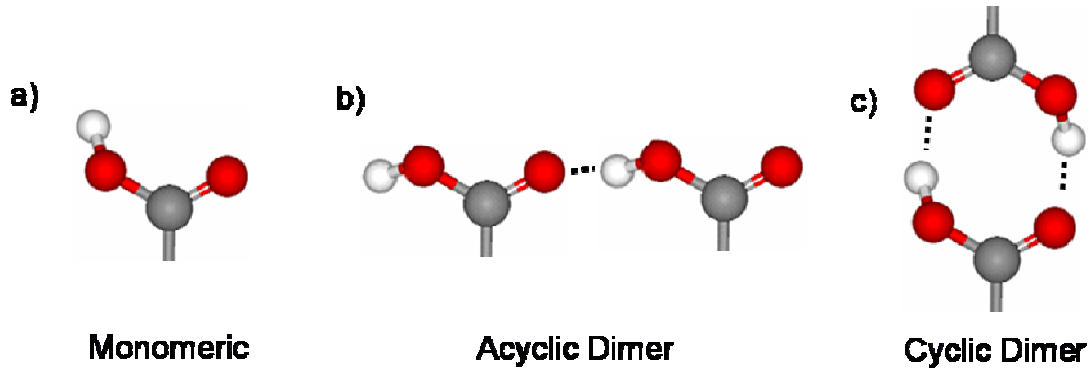

Figure 3.12. States of the carboxylic acid headgroup: (a) monomeric, (b) acyclic dimer and (c) cyclic dimer.

The cyclic dimer results from the interaction of 4-MBA molecules bound to the gold surface and unbound 4-MBA molecules, or other carboxylic acid molecules, from solution via two hydrogen bonds analogous to the structure reported for gas-phase benzoic acid [19, 20].

In Figure 3.13 we provide a typical reflectance absorption signal for 4-MBA covered-gold slides prepared from identical conditions used in the electrochemical experiments (1 mM 4-MBA in 95% ethanol for 24 hours, rinsed with Milli-Q water and dried in an Argon environment).

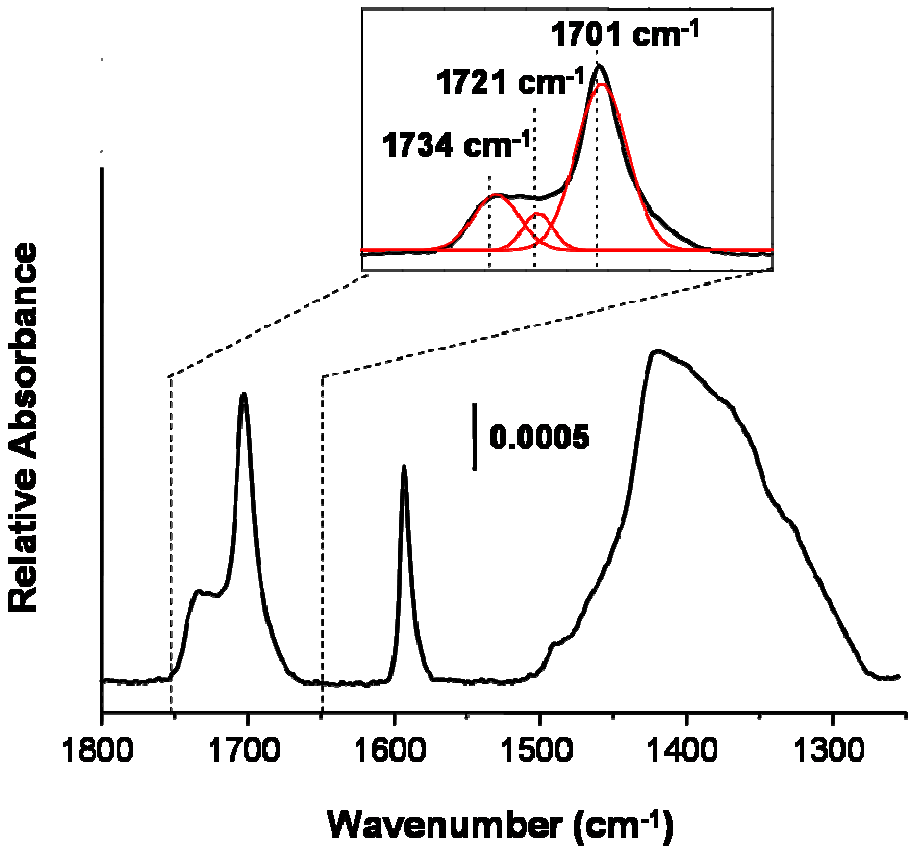

Figure 3.13. Representative ER-FTIR spectrum of a gold-coated silicon slide incubated in 1 mM 4-MBA ethanolic solution for 24 hours, rinsed with Milli-Q water and dried in an Argon environment.

Analysis of this sample spectrum reveals a sharp peak at 1590 cm^{-1} which is consistent with the C=C aromatic stretch of the benzene ring [15, 17]. There are two other regions we should note. We have already briefly mentioned the spectral region associated with the carboxylic acid moiety, 1750-1690 cm^{-1}, but we should also mention the broad spectral region between 1450-1350 cm^{-1} which is primarily comprised of symmetric CO_2^- stretches (1460-1400 cm^{-1}) and C-O-H deformations

(~1430 cm^{-1}) [15, 18, 21]. This last region is very difficult to characterize as it is strongly convoluted, however, some insight can be made following previous studies in the literature. The interpretation we provide in essence suggests that the presence of any signal in this region is evidence of at least some partially deprotonated species.

At the same time, we see strong evidence for COOH carbonyl stretching in our representative spectrum. If we perform a deconvolution of the 1750-1690 cm^{-1} spectral region (Figure 3.13) we see we have three contributing signals. These signals are predicted for the various hydrogen-bonded motifs mentioned above (Figure 3.12). Thus, it is evident from the infrared data that our incubation and rinsing procedure for 4-MBA SAMs gives rise to a heterogeneous structure with varying states of the carboxylic acid terminus.

It should be noted that on closer examination of the ER-FTIRS spectrum presented in Figure 3.13 that we do not see any evidence of the asymmetric carboxylate stretch typically found in the 1575-1500 cm^{-1} region [15]. Our result is not unlike the results obtained by Zangmeister and van Zee [21] for a very similar experiment, where an intense symmetric peak (~1425 cm^{-1}) but no evidence of the higher frequency asymmetric mode (1550 cm^{-1}) was reported. In our experiment, a 4-MBA SAM modified slide was exposed to a pH 9 solution. After exposure we managed to acquire a signal at 1550 cm^{-1} but it was substantially smaller compared to the symmetric COO^- stretch at 1425 cm^{-1}. This is in contrast to the research done by

Wells *et al.* where they show clear evidence of the 1550 cm^{-1} band after soaking a 4-MBA SAM in a pH 8.5 solution [15].

If we now consider the surface selection rules, previously discussed, we should be able to get some information about the conformation of the acid headgroups in a 4-MBA SAM. To do this, we will look closely at the relative absorption intensities of the symmetric and asymmetric modes for the carboxylate anion (COO^-) (Figure 3.14).

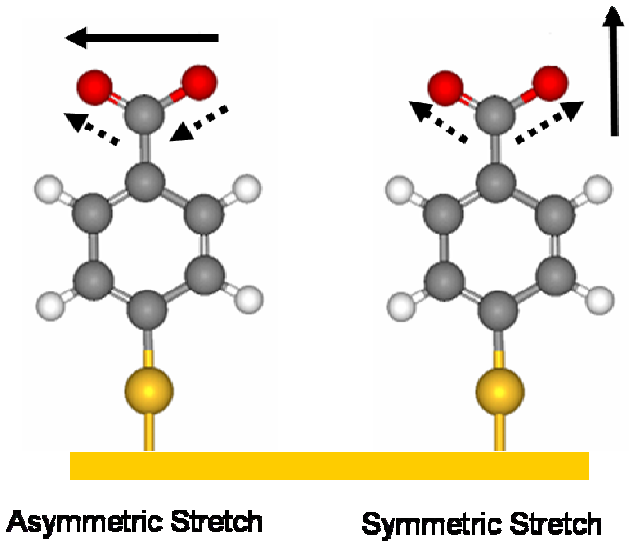

Figure 3.14. Transition dipole moments of the (a) symmetric and (b) asymmetric COO^- stretching vibration.

We know from the surface selection rules that only those modes that are perpendicular to the surface will be enhanced as they have transition dipoles aligned in the direction of the electric field vector of our IR radiation. To obtain the

maximum enhancement, p-polarized light at very shallow grazing angles are utilized. It is also known that the symmetric carboxylate stretch is perpendicular to the electrode, whereas the asymmetric is parallel. As such, data from IR measurements indicate that the planar carboxylate headgroup of 4-MBA is perpendicular to the gold substrate with little to no tilt. This result is indicative of a highly rigid monolayer with little flexibility about the C-C bond between the benzene backbone and the carboxylic acid moiety.

3.3.3 Cation Exchange Effect

As previously mentioned, we suspect that the attenuation of the peak current height was due to cation exchange between the electrolyte and the acid SAM headgroup. As shown earlier, an initial test of this behaviour was examined where we looked at two different concentrations of our NaF electrolyte. Those results (Figure 3.9) showed that the higher the concentration, the more rapid the attenuation. To further test this we ran a series of electrochemical experiments of 50 mM electrolyte solutions, all at the same pH, with different cations present.

The resulting CVs are presented, which are the second scans in all cases, in Figure 3.15 with $NaClO_4$, at a pH of 8.6 (panel a), $KClO_4$ at pH 8.3 (panel b) and $Ca(ClO_4)_2$ at pH 8.5 (panel c). We chose to use the second scans to allow one complete cycle of the potential region before our analysis. The pH of the various electrolytes was adjusted using either NaOH (panel a) or KOH (panels b, c).

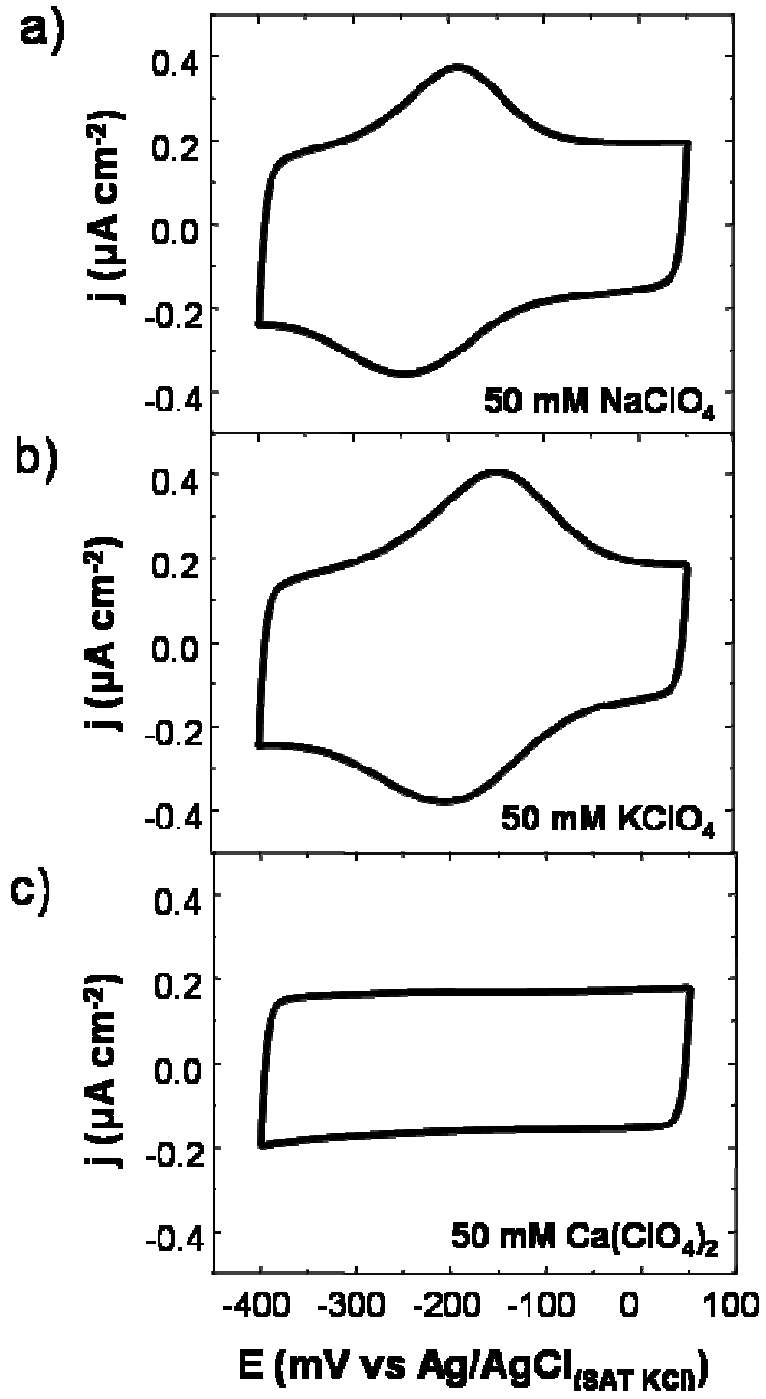

Figure 3.15. CVs of 4-MBA SAMs on polycrystalline gold electrodes in different electrolytes. (a) $NaClO_4$, at a pH of 8.6, (b) $KClO_4$ at pH 8.3 and (c) $Ca(ClO_4)_2$ at pH 8.5.

It should also be noted that $Mg(ClO_4)_2$ and $Ba(ClO_4)_2$ electrolytes were also used but presented identical results to the $Ca(ClO_4)_2$ experiment. From a qualitative analysis of the voltammograms run in the sodium and potassium perchlorate electrolytes, it is observed that the resulting curves are essentially the same. In both cases we clearly have a well defined pair of peaks and as in the case of the 50 mM NaF and NaPB electrolytes. We also see an attenuation of the peak as a function of immersion time in these electrolytes. When we look at the experiments involving the divalent cationic perchlorate electrolytes, we essentially see no indication of a peak whatsoever. Instead what we end up measuring is a voltammogram that resembles the charging envelope expected for an alkane thiol SAM.

Given this result, several experiments were tried using sodium perchlorate where small amounts of calcium perchlorate were spiked into the electrolyte solution. Throughout this experiment, CVs were measured and before the calcium was added we had voltammetric peaks that were slowly diminishing away in magnitude. After addition of the calcium, however, the voltammetric peaks vanished completely. Ultimately, in the presences of calcium ions, we see a rapid suppression of the electric-field driven protonation-deprotonation process. We conclude that the calcium ions are irreversibly binding to the carboxylate anion preventing any further protonation processes.

The effect of proton replacement by a metal ion has been well studied, going as far back as the work done by Langmuir and Schaefer, for acid monolayers formed

at the air-water interface [22]. Since those initial reports, there have been many subsequent studies on such monolayers where the relative strengths of proton displacement by various metal ions have been studied [23, 24, 25, 26]. From these studies, calcium ions form complexes with much larger binding constants compared to the heavier divalent cations. There have also been studies [27] that have reasoned that calcium is more strongly bound than sodium due to partial covalent character of the calcium-oxygen bond. This strong association of alkali metal ions and carboxylates could also result in appreciable changes in film structure as seen by Johann *et al.* where they suggest that structural changes in a fatty acid film structure as a function of pH could be the result of trace amounts of polyvalent metal ions in solution [28].

These ion-exchange effects have been studied on monolayers of acid thiols for a variety of cations using an assortment of surface sensitive techniques. Li *et al*. for instance have performed grazing incidence X-Ray Diffraction studies [25] that have shown cation overlayers can be formed by exposing carboxylic acid SAMs to solutions containing Ca^{2+} and Cd^{2+} ions. Burshtain and Mandler [23, 24] have studied Cd^{2+} ion binding to mercaptoalkanoic acid SAMs using electrochemical techniques to study the capacitance of the monolayers. It is also interesting to note that the data treatment used by Burshtain and Mandler is essentially an adaptation to the model proposed by Smith and White [1]. There have also been Quartz Crystal Microbalance (QCM) studies looking at the ion-exchange between the acidic protons of 4-MBA with Pb^{2+} and Cd^{2+} [29]. Based on QCM studies, Wang *et al.* suggest that

the pKa of the monolayer is largely independent of the counter ion's identity, which is in agreement with the double-layer capacitance titrations results done by Kakiuchi *et al* [30]. These authors suggest that sodium ions binding to the surface carboxyl groups result in screening the surface which might account for the counterintuitive observation that deprotonation is more favoured with increasing degree of dissociation within the acid SAMs.

Based on these reports of the behaviour of acid terminated Langmuir and self-assembled monolayers, we suggest that our electrochemical results are evidence of ion-exchange between the carboxylic acid protons and cations present in the electrolyte solution stopping the electric-field protonation-deprotonation process.

To lend further evidence to this cation exchange hypothesis, we preformed experiments where we analyzed the molecular effect on the 4-MBA SAMs by means of ER-FTIRS. In order to do this two gold coated slides with 4-MBA SAMs were prepared and measured their IR spectrum, using the bare-gold coated slide as a reference spectrum. Following this, the slides were exposed for two hours (the time spent in the electrolyte for our electrochemical experiments) in either 1 mM $NaClO_4$ or 1 mM $Ca(ClO_4)_2$ solutions. After, the slides were rinsed with water, dried in an Argon environment and the IR spectra were re-measured. From Figure 3.16, we can see that in both cases exposure to the electrolyte solutions caused an increase in the carboxylate IR band (~1425 cm^{-1}) suggesting the formation of a carboxylate salt.

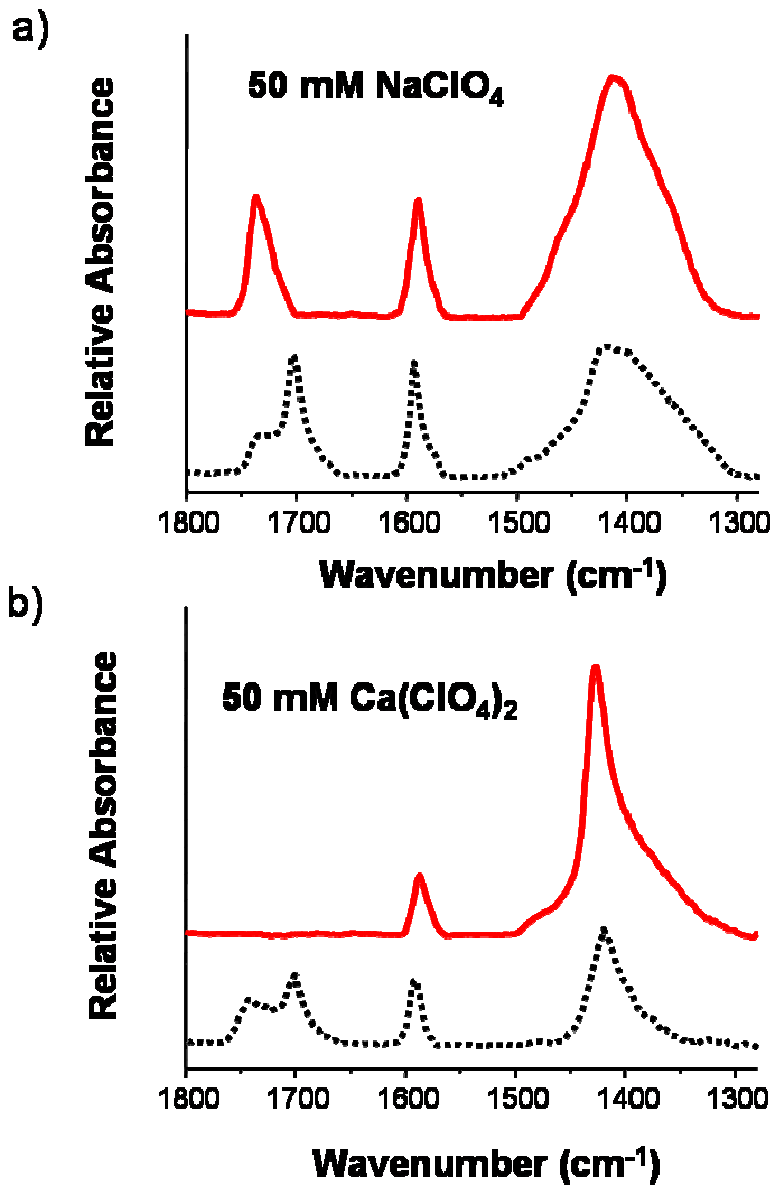

Figure 3.16. ER-FTIR spectra demonstrating the effect of exposing a 4-MBA SAM gold coated silicon slide in aqueous solutions containing: (a) 50 mM $NaClO_4$ and (b) 50 mM $Ca(ClO_4)_2$. The lower spectrum, in both panels, corresponds to the 4-MBA SAM before exposure to the respective electrolyte solutions (upper spectra).

The most pronounced change is found in the COOH carbonyl region of the spectra where we see dramatic differences between the two slides and the resulting SAM structures. The slide exposed to the calcium ions, Figure 3.16b, shows a complete loss of COOH carbonyl moieties whereas the sodium ion exposed slide shows an enhancement in the higher frequency (1740 cm^{-1}) carbonyl stretch with a decrease in the lower frequency (1700 cm^{-1}) stretch.

This implies that the sodium ions are disrupting the hydrogen-bonded network whereas the calcium ions completely destroy the network. This observation fits nicely with the electrochemical data where we see a complete loss of the voltammetric peak associated with the protonation-deprotonation process in the presence of calcium and a slow attenuation in the case of sodium. In the next section we will show that the presence of intermolecular hydrogen bonding COOH headgroups is correlated to the measured voltammetric peak in the electrochemistry.

3.3.4 Influence of Hydrogen Bonding

The infrared data clearly indicates that the formation conditions of our SAMs lead to a mixture of states for the 4-MBA carboxylic acid moiety (Figure 3.13). This observed assorted acid SAM structure has been attributed to the extensive hydrogen bonding [18, 31] and electrostatic effects [32] present within carboxylic acid monolayers. As such, various attempts have recently been made to minimize these effects, particularly decreasing the extent of hydrogen bonding, by the addition of

organic acids into the ethanolic incubating solution [18, 31, 33, 34]. One such example is the addition of acetic acid (AA). This has the effect of minimizing intermolecular hydrogen bonding between the acid SAM molecules as they become bonded to AA instead. Once the incubation is complete, the AA is presumably removed by copiously rinsing the gold substrate with water. It was important for the course of these experiments that we used ultra pure acetic acid instead of reagent grade. The reason being is that reagent grade AA contains larger amounts of calcium, and other divalent cations, which interfere with the protonation-deprotonation process as previously discussed.

Cyclic voltammetry and infrared experiments were performed in parallel to study the effects of adding AA (ultra pure, 5% by volume) to the incubation solution. Figure 3.17 compares the IR spectra of 4-MBA monolayers prepared from ethanolic solutions with and without AA. Looking first at the C=C aromatic stretching modes we notice that there is essentially little change between the two. However, we do start to see differences with all the other bands associated with 4-MBA. For instance we see that there is a decrease in the relative intensity associated with the COO^- symmetric stretch (~1400 cm^{-1}) with the addition of AA to the incubating solution and we assume a large increase in the C-O-H deformation mode. This is in agreement with the concept that we have fully protonated our surface by incubating in a very acid medium. Interestingly enough, we see a definite inversion of the relative IR signal strength between the cyclic (head-to-head) dimer (1700 cm^{-1}) and the monomeric protonated stretch at ~1735 cm^{-1} with the addition of AA to the

incubating solution. This suggests that we have effectively disrupted the hydrogen bonding network between SAM molecules.

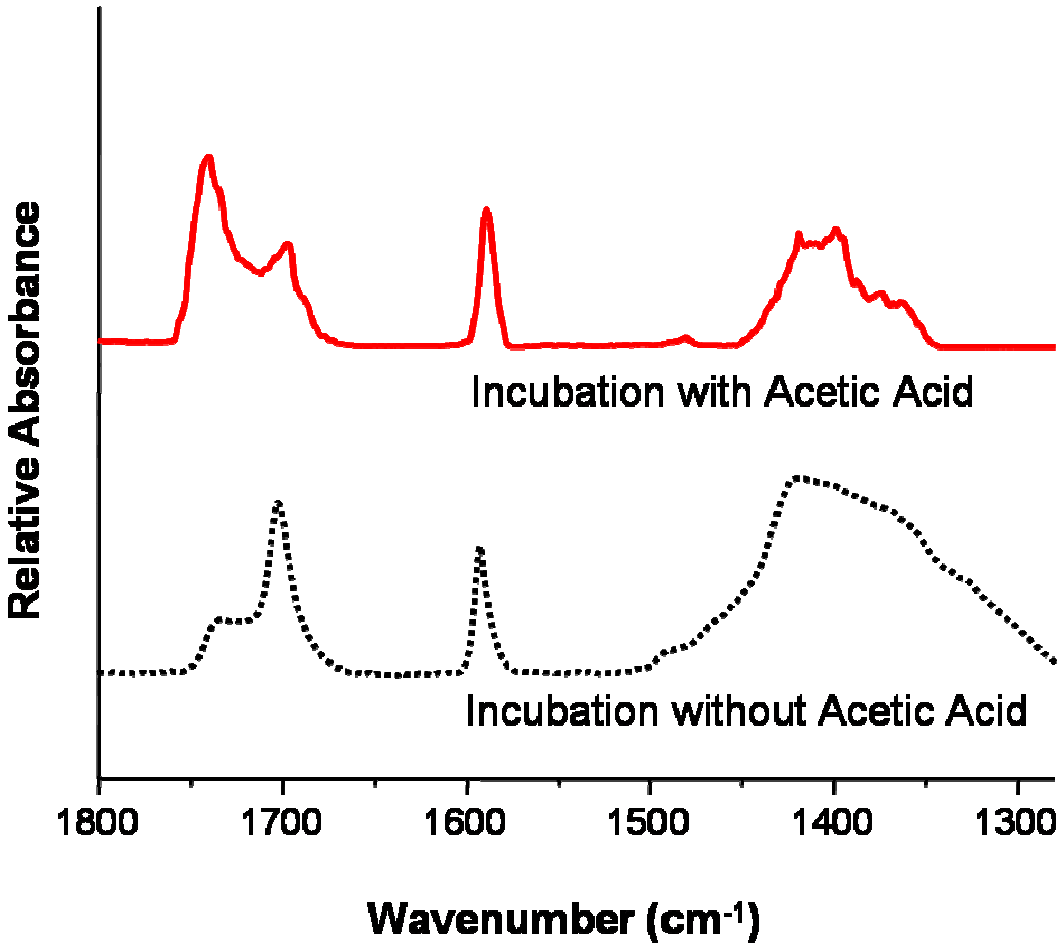

Figure 3.17. ER-FTIR spectra comparing the effects of 4-MBA SAMs on gold coated silicon slides prepared from 1 mM 4-MBA ethanolic solutions with 5% ultra pure acetic acid (upper spectrum) and without (lower spectrum).

However, we still see some infrared activity at ~1700 cm^{-1}, but it is quite possible that this signal is in fact due to AA being hydrogen bonded to the SAM and as such it does appear that addition of AA to the incubating solution attenuates the degree of hydrogen bonding between SAM molecules.

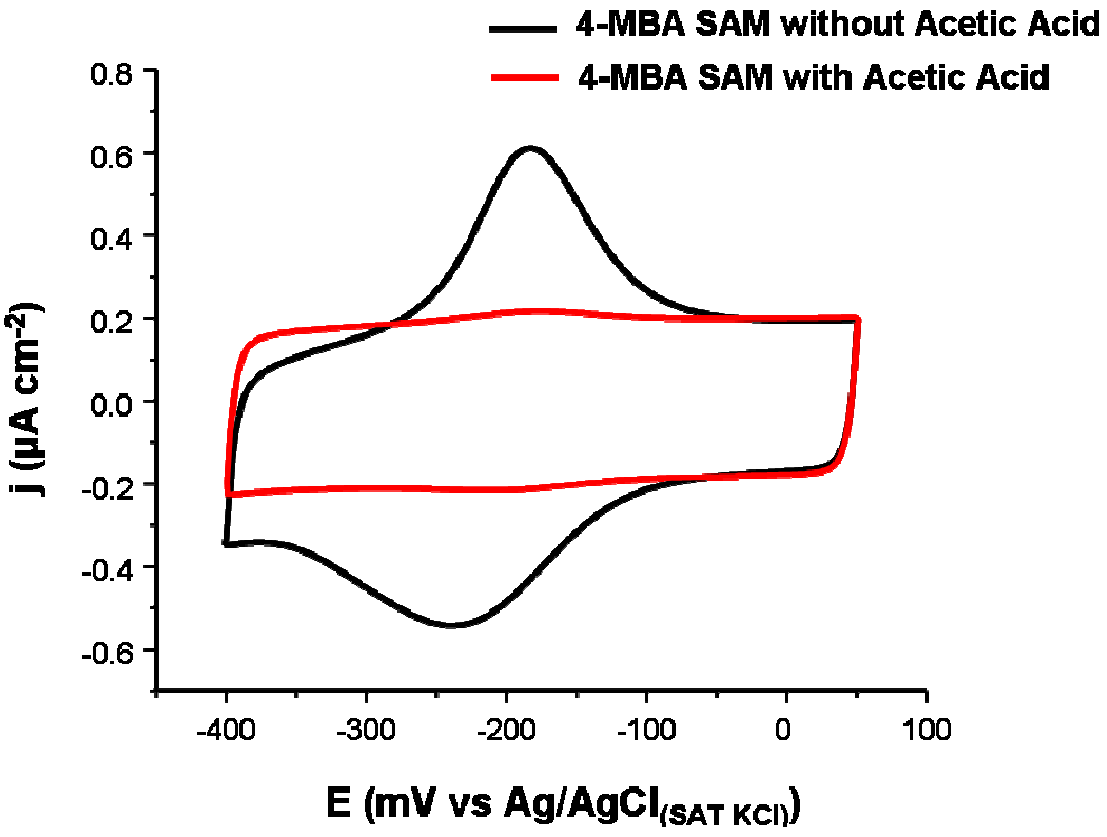

Figure 3.18. CVs comparing the effects of 4-MBA SAMs on gold coated silicon slides prepared from 1 mM 4-MBA ethanolic solutions with 5% ultra pure acetic acid (upper curve) and without (lower curve).

CVs were also obtained from gold electrodes incubated with and without AA for the various electrolytes previously discussed. From Figure 3.18, representative voltammograms, we can see that there is almost complete attenuation of the peaks associated with the protonation-deprotonation process for SAMs incubated with AA compared to those without AA. Given these electrochemical and infrared results, we conclude that hydrogen bonding is required for the observation of the electric-field driven protonation-deprotonation reaction.

3.4 Conclusions

We have been able to demonstrate that the carboxylic acid moiety of 4-MBA SAMs can be protonated and deprotonated by applying the appropriate potential to the SAM modified electrode surface, similar to MUA. From our measurements we have seen that in concentrated electrolyte solutions, this electric-field driven process slowly diminishes with increasing exposure of the SAMs to the electrolyte solution. We attribute this effect to an ion-exchange mechanism that causes disruptions in the intermolecular SAM hydrogen bonding network. The addition of calcium ions to the electrolyte cause an immediate suppression of the reversible protonation-deprotonation process as calcium irreversibly binds to form a carboxylate salt on the surface. These results were based on both electrochemical and *ex-situ* ER-FTIRS where we also examined the effect of incubating 4-MBA SAMs in the presence of ultra pure acetic acid. By combining the results from these experiments, we have been able to show that both ion-exchange and the disruption of the hydrogen bonding

network leads to the loss of the voltammetric signal attributed to the acid-base behaviour of the 4-MBA SAMs.

3.5 Reference

[1] Smith, C.P; White, H.S., *Langmuir* **1993**, *9*, 1.

[2] Burgess, I.; Seivewright, B.; Lennox, R.B., *Langmuir* **2006**, *22*, 4420.

[3] White, H.S.; Peterson, J.D.; Cui, Q.; Stevenson, K.J., *J. Phys. Chem. B* **1998**, *102*, 2930.

[4] Fawcett, W.R.; Fedurco, M.; Kovacova, Z., *Langmuir* **1994**, *10*, 2403.

[5] Bard, A.J.; Faulkner, L.R., *Electrochemical Methods Fundamentals and Applications, 2nd Edition*, Copyright **2001** John Wiley & Sons, Inc., New York, New York, pp. 239.

[6] Ingle, J.D. Jr.; Crouch, S.R., *Spectrochemical Analysis*, Copyright **1988** Prentice-Hall, Inc., Upper Saddle River, New Jersey, pp. 404.

[7] Ingle, J.D. Jr.; Crouch, S.R., *Spectrochemical Analysis*, Copyright **1988** Prentice-Hall, Inc., Upper Saddle River, New Jersey, pp. 412.

[8] Skoog, D.A.; Leary, J.J., *Principles of Instrumental Analysis, 4th Edition*, Copyright **1992** Saunders College Publishing, New York, New York, pp. 252.

[9] Harris, D.C.; Bertolucci, M.D., *Symmetry and Spectroscopy An Introduction to Vibrational and Electronic Spectroscopy*, Copyright **1989** Dover Publications, New York, New York, pp. 93.

[10] Ingle, J.D. Jr.; Crouch, S.R., *Spectrochemical Analysis*, Copyright **1988** Prentice-Hall, Inc., Upper Saddle River, New Jersey, pp. 406.

[11] Chazalviel, J.-N.; Ozanam, F. in Alkire, R.C.; Kolb, D.M.; Lipkowski, J.; Ross, P.N. (Eds.), *Advances in Electrochemical Science and Engineering, Vol. 9*, Wiley-VCH Verlag GmbH & Co. KGaV, Chichester, UK, **2006**, pp. 199.

[12] Arihara, K.; Ariga, T.; Takashima, N.; Arihara, K.; Okajima, T.; Kitamura, F.; Tokuda, K.; Ohsaka, T., *Phys. Chem. Chem. Phys.* **2003**, *17*, 3758.

[13] Malem, F.; Mandler, D., *Anal. Chem.* **1993**, *65*, 37.

[14] Giz, M.J.; Duong, B.; Tao, N.J., *J. Electroanal. Chem.* **1999**, *465*, 72.

[15] Wells, M.; Dermody, D.L.; Yang, H.C.; Kim, T.; Crooks, R.M., *Langmuir* **1996**, *12*, 1989.

[16] Nuzzo, R.G.; Dubois, L.H.; Allara, D.L., *J. Am. Chem. Soc.* **1990**, *112*, 558.

[17] Smith, E.L.; Alves, C.A.; Anderegg, J.W.; Porter, M.D., *Langmuir* **1992**, *8*, 2707.

[18] Arnold, R.; Azzam, W.; Terfort, A.; Wöll, C., *Langmuir* **2002**, *18*, 3980.

[19] Bakker, J.M.; Aleese, L.M.; von Helden, G.; Meijer, G., *J. Chem. Phys.* **2003**, *119*, 11180.

[20] Stepanian, S.G.; Reva, I.D.; Radchenko, E.D.; Sheina, G.G., *Vib. Spectrosc.* **1996**, 11, 123.

[21] Zangmeister, C.D.; van Zee, R.D., *Langmuir* **2003**, *19*, 8065.

[22] Langmuir, I; Schaefer, V.J., *J. Am. Chem. Soc.* **1936**, *58*, 284.

[23] Burshtain, D.; Mandler, D., *Chem. Phys. Chem.* **2004**, *5*, 1532.

[24] Burshtain, D.; Mandler, D., *J. Electroanal. Chem.* **2005**, 581, 310.

[25] Li, J.; Liang, K.S.; Scoles, G.; Ulman, A., *Langmuir* **1995**, 11, 4418.

[26] Sastry, M.; Patil, V.; Mayya, K.S., *J. Phys. Chem. B* **1997**, 101, 1167.

[27] Webb, D.A.; Danielli, J.F.; *Nature* **1940**, 146, 197.

[28] Johann, R.; Vollhardt, D.; Möhwald, H., *Colloids Surf. A* **2001**, 182, 311.

[29] Wang, J.; Frostman, L.M.; Ward, M.D., *J. Phys. Chem.* **1992**, 96, 5224.

[30] Kakiuchi, T.; Iida, M.; Imabayashi, S.; Niki, K., *Langmuir* **2000**, 16, 5397.

[31] Wang, H.; Chen, S.; Li, L.; Jiang, S., *Langmuir* **2005**, *21*, 2633.

[32] Sushko, M.L.; Shluger, A.L., *J. Phys. Chem. B* **2007**, 111, 4019.

[33] Dannenberger, O.; Weiss, K.; Himmel, H.-J.; Jager, B.; Buck, M.; Woll, C., *Thin Solid Films* **1997**, *307*, 183.

[34] Willey, T.M.; Vance, A.L.; van Buuren, T.; Bostedt, C.; Nelson, A.J.; Terminello, L.J.; Fadley, C.S., *Langmuir* **2004**, *20*, 2746.

4 Analysis of 11-Mercaptoundecanoic Acid Self-Assembled Monolayers by *in-situ* Spectroelectrochemical Fourier Transform Infrared Spectroscopy

4.1 Introduction

Although the level of information that can be acquired through electrochemical techniques is substantial, the molecular structure at the electrified interface can only be inferred without the further aid of spectroscopy. Several questions arise when trying to analyze self assembled monolayers (SAMs) using *ex-situ* techniques, such as External Reflectance - Fourier Transform Infrared Spectroscopy (ER- FTIRS). How does the loss of potentiostatic control affect the SAM? How much does the structure of the SAM change after being dried and not in contact with an electrolyte? What role does contamination play from having to transfer samples between instruments? What state of protonation of the film do we have on either side of the voltammetric

peak associated with the electric-field driven protonation-deprotonation process? To fully understand the behaviour of switchable surfaces these are important questions to consider. As such, there have been numerous attempts to combine molecular spectroscopy with electrochemistry to try and develop a full picture of what is a happening at these electrified interfaces. To this end, several common approaches to the problem include optical ellipsometry [1], surface enhanced Raman spectroscopy [2], infrared (IR) spectroscopy [3, 4, 5, 6, 7], second harmonic and sum frequency generation [8, 9].

Of particular interest in the field is the use of infrared reflection-absorption spectroscopy (IRRAS). In this technique there are essentially two modes of operation, internal and external reflectance (Figure 4.1). The later technique has the

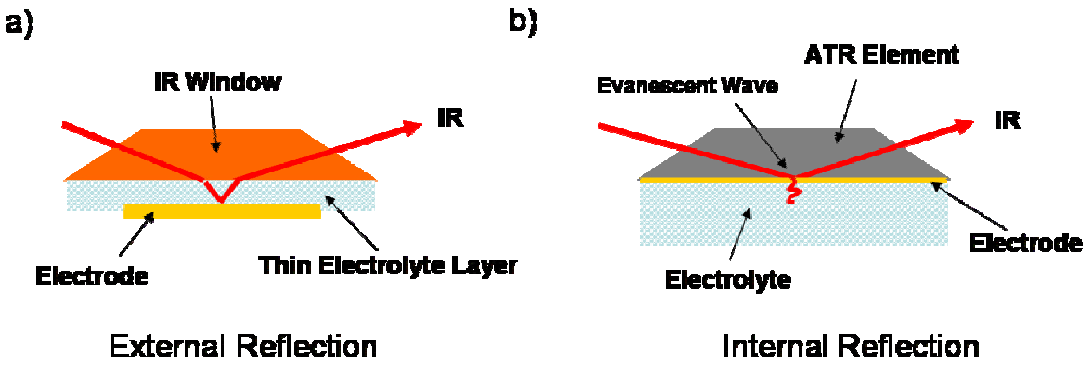

Figure 4.1. Generalized schematic diagrams showing the difference between (a) external reflection and (b) internal reflection infrared reflection-absorption spectroscopy techniques.

IR radiation passing through an IR window crosses through a very thin layer of electrolyte where the radiation makes a single reflection off the electrode interface. Although this technique is relatively simple to setup, it has several major drawbacks. The most significant for the longest period of time prevented significant advancement in the field [10], is the absorption of IR radiation by the electrolyte which tends to be orders of magnitude stronger than the absorption by the molecules of interest. To try and minimize this effect and to gain valuable insight into the molecular structure of adsorbed molecules on the electrified interface a popular method is to minimize the thickness of the electrolyte near the interface. This is achieved by pressing the electrode against the IR window. Still, we have to keep in mind that the IR radiation is not only going to interact with the molecules adsorbed at the interface, but it has the potential to interact with unbound molecules in the electrolyte. Various techniques try to circumvent this, an example being Polarization Modulation Infrared Reflectance Adsorption Spectroscopy (PM-IRRAS) [11], by modulating the polarization of the incident radiation to gain insight into the interface. However, external reflectance techniques, with the electrode pressed against an IR window, create electrochemistry problems due to large electrolyte resistances in the thin-layer cavity and greatly reduced mass transport.

To overcome the issue of strong absorption levels of the electrolyte, one can switch from an external to internal reflectance technique. As demonstrated by Figure 4.1(b) the incident IR radiation impinges on a prism made from an infrared transparent material and internally reflects off the interface of interest. As a

consequence of this reflection, an evanescent wave is formed that extends beyond the plane of reflection of the prism and interacts with molecules present at the interface. This then provides valuable insight into the molecular structure at the interface. By switching to an internal reflectance experimental setup, we can effectively eliminate the complications of IR absorption due to the electrolyte and still effectively analyze those molecules bound to the surface.

In an effort to try and complete the picture of the electric-field driven protonation-deprotonation reactions of carboxylic acid terminated SAMs, 11-mercaptoundecanoic acid (MUA) was studied utilizing an *in-situ* internal reflection-absorption infrared technique. The decision to use MUA over 4-MBA was due to difficulties in preparing the 4-MBA SAM in the *in-situ* electrochemical cell. MUA proved to be a much easier monolayer to build than 4-MBA and was a suitable 'proof of concept' system as both molecules show similar electrochemistry with the protonation-deprotonation reaction.

4.1.1 *in-situ* Spectroelectrochemical Attenuated Total Internal Reflection Fourier Transform Infrared Spectroscopy

Attenuated Total Reflectance (ATR) is a sampling technique that can be used with infrared spectroscopy for the analysis of solids and liquids. It has advantages over other sampling techniques in that a sample, either liquid or solid, can be readily analyzed without further preparation [12]. This is achieved by using a property of the

total internal reflection phenomenon, called an evanescent wave. When total internal reflection occurs an electromagnetic wave, the evanescent wave, extends beyond the reflecting surface into the sample. [12]

Using ATR as the sampling mode for FTIR requires a beam of infrared radiation to impinge on a prism of infrared transparent material (Si and ZnSe are suitable examples) in such a way that there is a reflection off at least one internal surface of the crystal. At this point of reflection, an evanescent wave is formed and extends beyond the surface of the crystal into the sample a distance that is dependent on the wavelength of light and the refractive index of the medium [12]. Naively, one would expect that the interface acts as a simple mirror reflecting the wave. However, if we apply Maxwell's equations to this scenario, a solution does not exist without the addition of a transmitted wave through the interface called an evanescent wave. The evanescent wave can then be absorbed by molecules in close proximity to the surface. In the case of infrared radiation this absorption causes vibrational excitations of the chemical bonds within these molecules (following the surface selection rules mentioned in the previous chapter). The attenuated reflected beam then exits the crystal and is measured by a detector.

In the case of our *in-situ* spectroelectrochemical ATR FTIR instrument, we first set up the FTIR spectrometer with an ATR crystal in the vertical Kretshmann configuration with a thin layer of plated gold, to be used as an electrode, on the reflecting plane of the ATR element. Sealing the ATR crystal in an electrochemical

cell we can now control the potential of the electrode and acquire the molecular structure of the interface, while maintaining potential control, on the surface using an ATR-FTIR sampling technique.

4.1.1.1 Subtractively Normalized Interfacial Fourier Transform Infrared Spectroscopy

A popular method to isolate potential-sensitive infrared absorption through an *in-situ* spectroelectrochemical technique is Subtractively Normalized Interfacial Fourier Transform Infrared Spectroscopy (SNIFTIRS) which was first described by Pons and Bewick [13]. This is a differential technique as it involves alternating the potential of the working electrode from a reference to a sample potential and then calculating the difference between the respective measured infrared spectra.

A unique feature of this technique is that the difference spectrum calculated between the sample and the reference is then normalized to the reference spectrum to account for any drift in the instrument. This allows for experiments to be run over extended periods of time without worrying about introducing artifacts into the data due to the drift. However, for this last statement to be true, the number of averaged infrared scan measurements for a given reference-sample read cycle must be kept small, putting any instrumental drift on the time scale of minutes. This unfortunately greatly reduces the signal to noise ratio of a given sample. To try and improve the signal to noise ratio, the cycle of measuring the reference and the sample spectra is

repeated *m* times until a total of $N = n \times m$ single beam spectra have been measured. Once all the spectra have been acquired, the co-added reference spectrum can be subtracted from the co-added sample spectrum with the result then normalized to the co-added reference spectrum for analysis. Mathematically, this can be defined as follows:

$$\frac{\Delta R}{R} = \frac{\left(R_E - R_{E_0}\right)}{R_{E_0}} \qquad \text{(Equation 4.1)}$$

where R_E and R_{E_0} are the co-added infrared single beam spectra at the sample and reference potentials respectfully. For this study, values of *n* and *m* employed were 128 and 4 respectfully for a total of 512 co-added single beam measurements at each potential providing adequate signal to noise ratios for data analysis. It should also be noted that data acquisition of the infrared spectra were delayed by 60 seconds after switching the potential. This delay allows for the interface to reach thermodynamic equilibrium at the new applied potential.

4.2 Experimental

Reagents, Solutions and Electrode Materials

11-Mercaptoundecanoic acid (95%), sodium fluoride (99.99%), sodium hydroxide (+98%), ammonium fluoride (+98%), sodium sulfite (+98%), sodium

thiosulfate (99%) and hydrogen tetrachloroaurate III (99.9%) were purchased from Sigma Aldrich and were used as received. All aqueous solutions were prepared from Milli-Q (>18.2 MΩ cm^{-1}) water. Ethanol (95%) was purchased from Commercial Alcohols Inc. (Brampton ON, CA). The procedure for fabricating the bead electrode from gold wire purchased from Alfa Aesar (99.95%) has been described in the previous chapter.

Electroless Deposition of Gold onto Silicon Hemispherical Prism

The general procedure we followed for deposition of gold onto the silicon hemispherical prism is reported elsewhere by Osawa *et al* [14]. We also adopted a slight modification described by Delgado *et al* [15]. The reflecting plane of a 25 mm diameter, non-doped, silicon hemispherical prism (Harrick Scientific Products, Pleasantville NY, US) was successively polished with finer grade diamond suspensions (Leco Corporation, St. Joseph MI, US) down to 0.5 μm. The prism was then degreased by sonication in ethanol and finally rinsed in Milli-Q (>18.2 MΩ cm^{-1}) water before deposition. To remove the oxide layer and to terminate the silicon surface with hydrogen, the reflecting surface was left in contact with 40% (w/w) solution of NH_4F for five minutes. The gold deposition was done at 55°C by dropping a solution containing 5 mg $HAuCl_4$, 0.3 M Na_2SO_4, 0.1 M $Na_2S_2O_3$, 0.1 M NH_4Cl and 2% HF (2:1 in volume) directly onto the polished face of the silicon hemispherical prism. After 80 seconds the gold deposition was quenched by rinsing the prism with copious amounts of Milli-Q (>18.2 MΩ cm^{-1}) water.

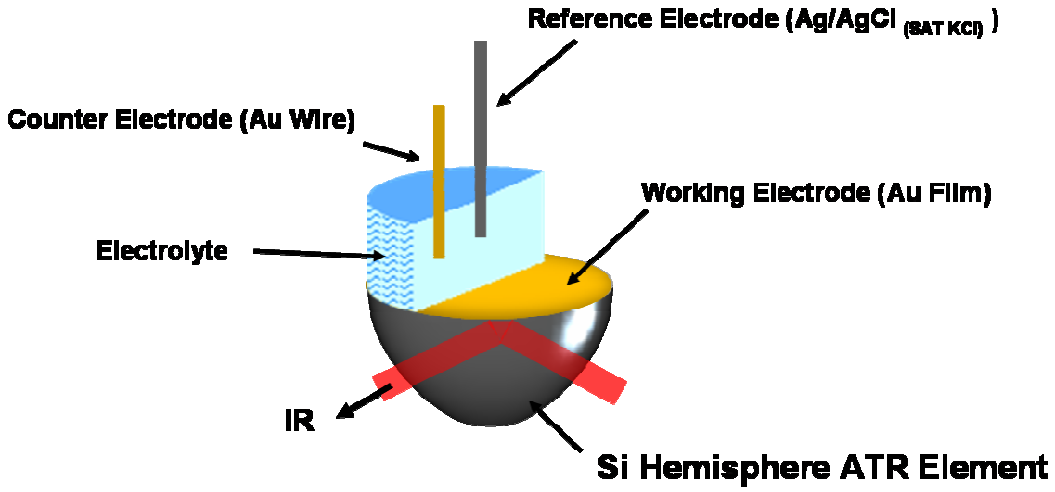

Figure 4.2. Schematic showing the general setup for our *in-situ* spectroelectrochemical ATR-FTIR measurements.

in-situ spectroelectrochemical ATR-FTIR Measurements

Our ATR-FTIR measurements were performed using an experimental set-up adapted from previous reports [16]. Briefly, a Teflon™ spectroelectrochemical cell in the vertical Kretshmann configuration was employed. The cell was constructed *in-house* and was equipped with a reference electrode (Ag/AgCl, saturated KCl) connected *via* a glass salt bridge. Electrical contact was made to the working electrode by pressing a coiled loop of gold wire against the Au-plated surface of the Si hemisphere. The counter electrode was a coil of gold wire, flame annealed before immersing into the working cell and electrolyte. The general setup for the ATR-FTIR apparatus is depicted in Figure 4.2.

Potential control was maintained using a PAR 173 (EG & G Princeton Applied Research) potentiostat and custom software written in LabVIEW (National Instruments). The electrolyte was deaerated by purging with argon for 30 minutes and a continual blanket of argon was maintained over the electrolyte throughout the experiment. The pH of the electrolyte was adjusted using either KOH or $HClO_4$. All ATR-FTIR spectra were measured using p-polarized incident radiation at 70^o with respect to the normal of the ATR element. A Nicolet 6700 Fourier Transform Infrared (FTIR) Spectrometer equipped with a mercury cadmium telluride (MCT) liquid nitrogen cooled detector was used to make the IR measurements at a resolution of 4 cm^{-1}. The sample chamber of the spectrometer was purged throughout the experiment using CO_2 and H_2O free air supplied by a Parker Balston FT-IR Purge Gas Generator 75-62 (Parker Hannifin Corporation, Haverhill, MA, US).

Self-Assembled Monolayer Preparation

The monolayer of 11-mercaptoundecanoic acid (MUA) was prepared for both the electrochemical and ATR-FTIR experiments in an identical manner. The monolayer was formed by incubating either the gold plated silicon hemisphere or a polycrystalline gold bead electrode in a 1 mM ethanolic solution for 24 hours. The substrate was then removed from the incubating solution and the monolayer rinsed with chilled ethanol before being dried in an argon atmosphere for 30 minutes.

Electrochemical Measurements

Cyclic voltammetric measurements were performed in an all-glass sealed cell, using a three electrode arrangement, which was connected to an external reference electrode (Ag/AgCl, saturated KCl) *via* a salt bridge. The counter electrode was a coil of flame annealed gold wire. Electrolytes were deaerated with argon with a continual blanket maintained above the electrolyte during all electrochemical experiments. All glassware was heated in a mixture of H_2SO_4 and HNO_3 (2:1 by volume) and then copiously washed and soaked overnight in Milli-Q (>18.2 MΩ cm^{-1}) water prior to every experiment. Data collection from a HEKA Potentiostat PG590 (HEKA, Mahone Bay, NS, Canada) was done using a multifunction DAQ card (PCI 6251 M Series, National Instruments Corporation, Austin, TX, USA) and in-house software written in the LabVIEW (National Instruments Corporation, Austin, TX, USA) environment.

4.3 Results

As previously mentioned, we had some technical problems studying 4-MBA SAMs using our *in-situ* spectroelectrochemical cell. The main issue was that during the incubation process our gold film on the silicon hemisphere delaminated. Without the gold film firmly affixed to the silicon hemisphere, we would not be able to get the required IR enhancements that we need to do this study. As such we moved to a

different chemical system, MUA, which showed similar electrochemical behaviour as 4-MBA and we could incubate it in our cell.

4.3.1 Electrochemical Results

To assist in the interpretation of the spectroscopic data and for comparison to the electrochemical results discussed for 4-MBA, similar electrochemical studies were done using MUA on polycrystalline gold. Figure 4.3 (a) shows a typical cyclic voltammogram (CV) for a MUA SAM in 1 mM NaF (pH 8.3 – adjusted using NaOH). The results of these studies are consistent with those discussed by Burgess *et al.* [16] showing the dependence of the carboxylic acid moiety with electrolyte pH and applied potential. From Figure 4.3 (b) we can see a similar peak (attributed to the protonation-deprotonation process) to that found in an identical experiment using SAMs formed from 4-MBA as discussed in the previous chapter.

The striking difference between the two is the magnitude of the measured currents. This is of no surprise if we consider the structural backbone differences between the two molecules. As mentioned in the previous chapter, MUA has a longer aliphatic tail compared to that of 4-MBA which leads to a substantially smaller inner layer capacity, modeling the interface as a Helmholtz capacitor, and subsequently a much smaller current is measured.

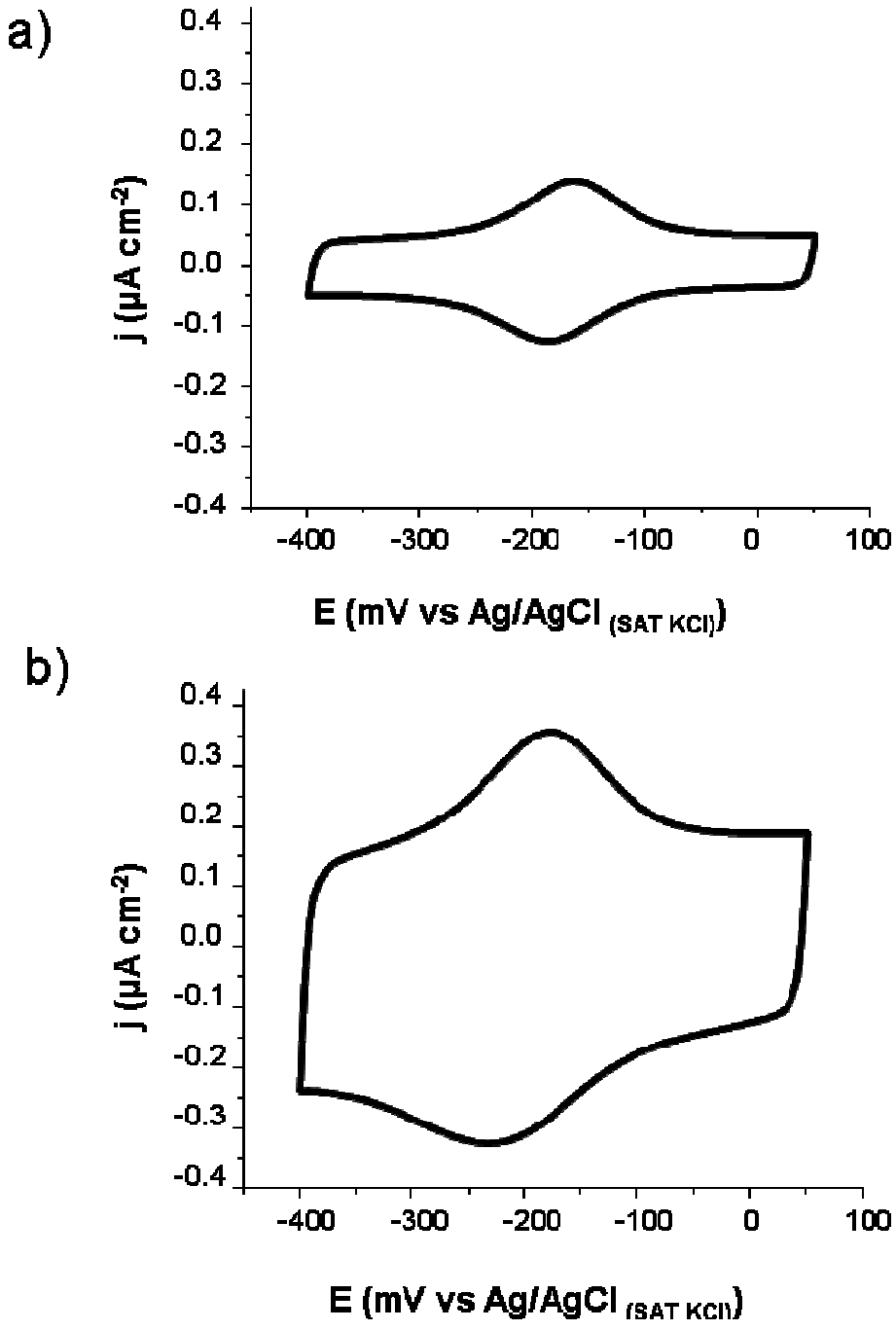

Figure 4.3. Electrochemical characterization of (a) MUA and (b) 4-MBA self-assembled monolayers formed on polycrystalline gold electrodes in 1 mM NaF (pH 8.3 – adjusted using NaOH) at a scan rate of 20 mV/s.

Another important feature in the CVs shown in Figure 4.3 is that there is a difference in magnitude of the inner layer capacities on each side of the potential peak. This may be explained by noting that on either side of the peak the state of the film is protonated or deprotonated. If the interface is modeled as a simple Helmholtz capacitor, we should see a difference in the dielectric constants on either side of the peak as well. Using a simple electrostatics argument the deprotonated species has a larger dielectric constant compared to the protonated state due to electrostatic interactions and hence differences in the measured inner layer capacity at potentials on either side of the peak. From this observation we can state that at potentials positive of the peak we have the protonated state (as the inner layer capacity is smaller) and for negative potentials we have the deprotonated state of the MUA SAM.

4.3.2 Subtractively Normalized Interfacial Fourier Transform Infrared Spectroscopy Results

The first step in probing the electric-field driven protonation-deprotonation nature of a carboxylic acid SAM by means of *in-situ* FTIR, was to determine what the various states of protonation of these surfaces look like as a function of pH. To do this an incubated SAM was exposed to a solution of low and high pH. Using Equation 4.1 we can determine normalized differences at the two different pHs by using an intermediate (pH 8 in this case) as the reference spectrum (Figure 4.4). We are able to use the same data treatment we use for the potential dependent

perturbations as we are effectively perturbing the interface by adjusting the environmental conditions in a controllable manner. The results give us an idea of what we should expect experimentally when we attempt to adjust the monolayer's state of protonation using electric fields.

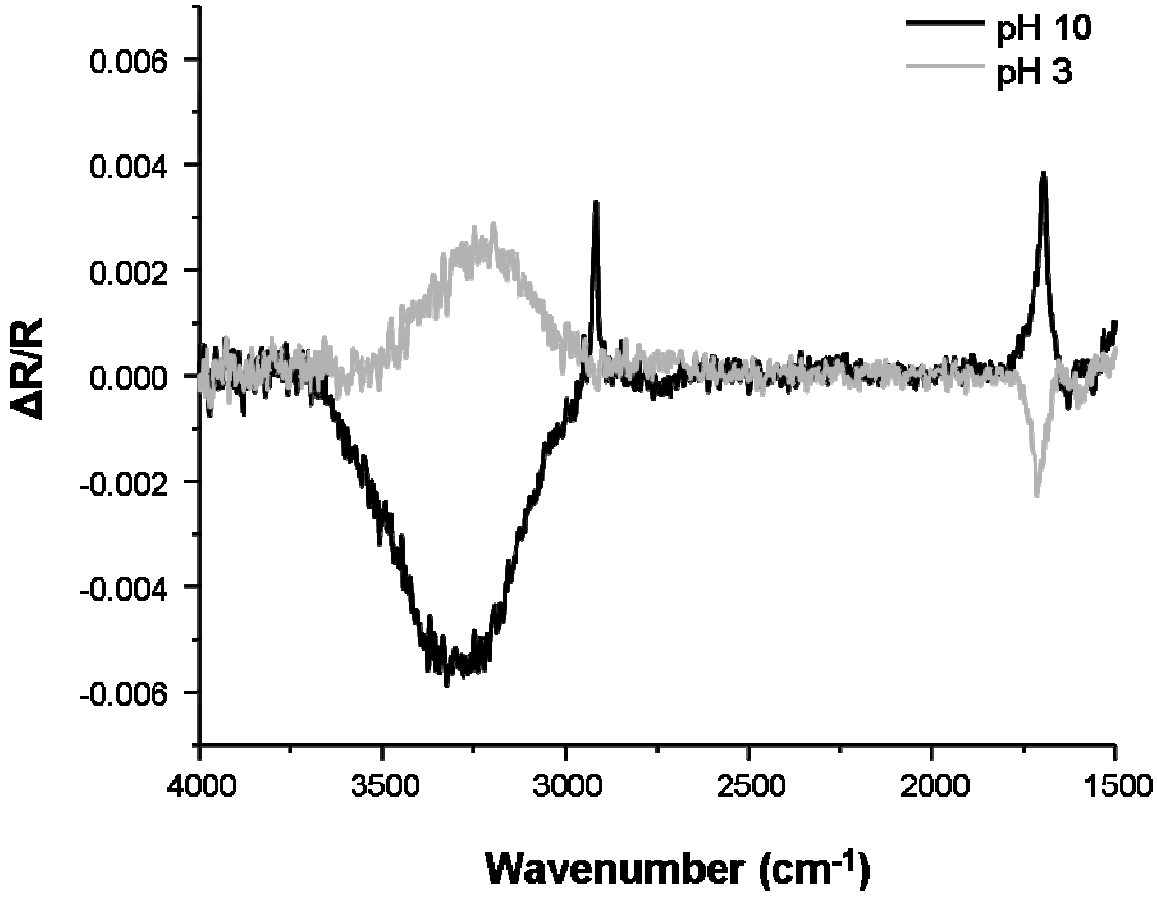

Figure 4.4. SNIFTIR spectra of MUA SAMs on gold coated silicon hemisphere using a measured spectrum at pH 8 as the reference spectrum. The MUA SAM was exposed to solutions of (a) pH 3 and (b) pH 10 for sample spectra measurements.

From Figure 4.4 we can see several differences between the spectrum measured at pH 3 and that of pH 10. Of particular interest is the area of the spectra around 1710 cm^{-1} which is associated with the carboxylic acid moiety [17, 18, 19, 20]. When attempting to analyze the spectra presented in Figures 4.4 (and 4.5) we first have to realize that a down going spectral feature is an indication of an increase in spectral intensity compared to the reference and vice versa for an upward going spectral feature (a loss of intensity relative to the reference). With this in mind, we see that we have both upward and downward going bands present. From Figure 4.4 we can see that at pH 3 we have an increase in the IR absorption of the carboxylic acid moiety of our MUA SAM. This is to be expected as at low pH the acid SAM should be fully protonated. The same holds true for high pH where we expect the SAM to be deprotonated which is evident by the loss of the carboxylic acid IR absorption at 1710 cm^{-1}. The broad spectral features around 3200 cm^{-1} are related to the structure and concentration of water at the interface. Increasing the pH leads to a larger water signal which is consistent with a more polar interface resulting from monolayer deprotonation [21]. The final interesting feature is the IR absorption signal at 2910 cm^{-1} indicating a change in the CH stretching vibration of the MUA alkane chain [20].

With this information now in hand, we have a handle of what the various extreme cases of protonation and deprotonation look like for an MUA SAM. The next step is to start applying various potentials to try and induce protonation-deprotonation of the SAM under fixed pH conditions. For these experiments we

selected a reference potential to be +50 mV vs Ag/AgCl and the stepped potential to be -400 mV vs Ag/AgCl as these potentials are on either side of the voltammetric peak in pH 8.5. At these potentials the state of the carboxylic acid moiety should differ and no other voltammetric processes, as previously discussed, should interfere with these measurements.

From Figure 4.5, we can see from our preliminary potential perturbation experiments we have indeed induced some molecular changes at the surface. In the case of the potential driven perturbations, the changes in the IR absorptions in the interface region occur in various ways. For instance, it may be a change in the concentration of some species due to adsorption/desorption. In the case of studying a redox molecule there is also the possibility of a Faradaic process occurring. As such, the interpretation of the data can be rather complicated.

Looking at Figures 4.5 once more, we see we have two negative going infrared bands (~3500 cm^{-1} and ~1620 cm^{-1}) for the spectrum obtained at -400 mV which correspond nicely to the OH stretching and HOH bending (or scissor HOH) modes of H_2O, water, respectfully [21]. The observation that these bands are both negative going as previously mentioned indicates that we have an increase in intensity of the IR absorptions of these modes. The likely cause of this increase is a change in the orientation of the H_2O molecules near the surface or an increase in their surface concentration. Again, this implies a more hydrophilic surface consistent with carboxylate rather than carboxylic acid termination.

The IR bands located around ~2910 cm^{-1} are attributed to the CH bond stretching modes of the long alkane chain in MUA [20]. It is interesting to note that these bands are positive indicating that there is a decrease in the measured surface signal. We can rule out the possibility that the decrease in surface signal is a

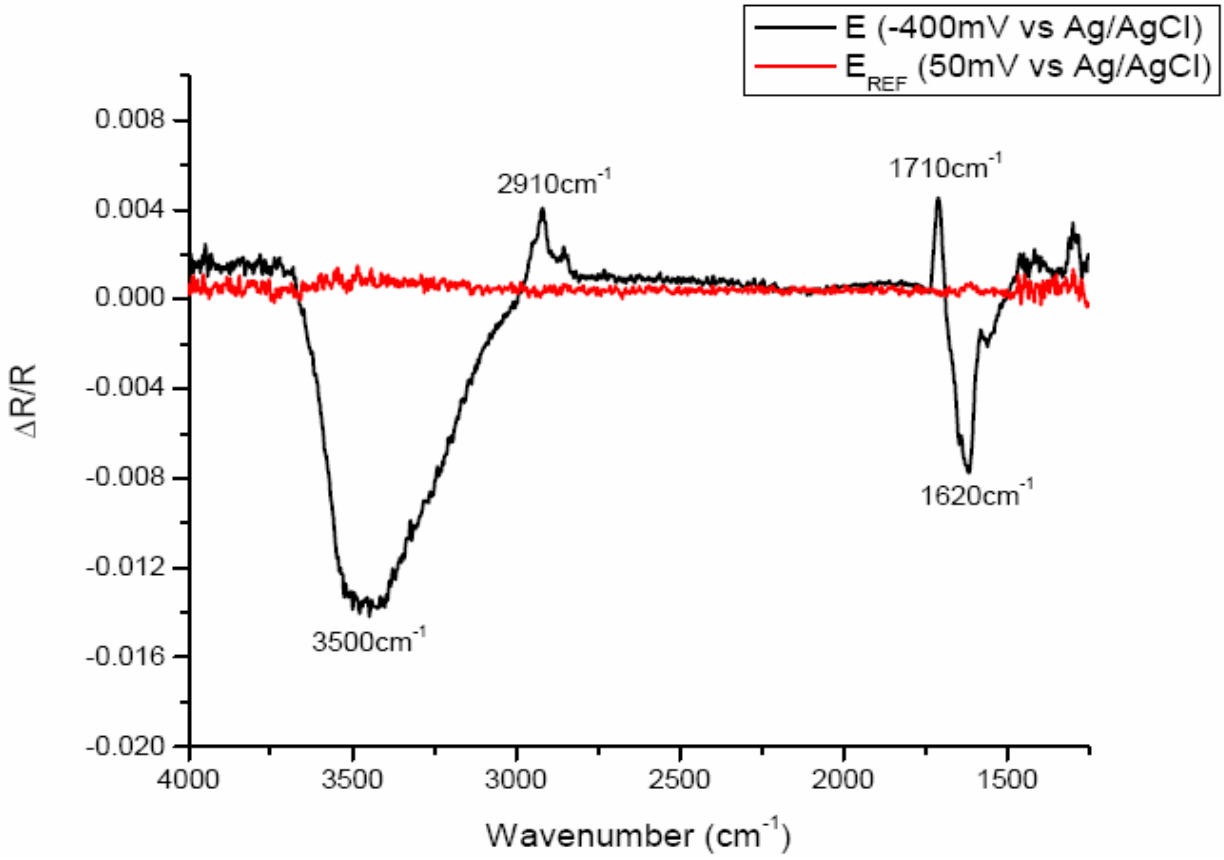

Figure 4.5. Preliminary SNIFTIR Spectroscopic potential perturbation experiments of MUA SAMs prepared on a gold coated silicon hemisphere measured in our *in-situ* spectroelectrochemical cell.

result of losing MUA molecules from the interface as the applied potential at which this spectrum is measured at (-400 mV versus Ag/AgCl) is more positive than the desorption potential (-600 mV versus Ag/AgCl) of MUA [16]. A possible explanation for this behaviour could be that there is a slight rearrangement of the film in the form of a tilted alkane backbone in MUA. Subsequently, this potential driven tilt would cause the electric dipole associated with the CH stretching mode to become less aligned with the associated infrared perturbation attenuating the absorption of IR radiation compared to the un-tilted molecule.

An explanation for this tilt could be the result of changes in the electrostatics at the SAM-electrolyte interface. If the SAM was to become deprotonated there would be a larger negative charge on the SAM side of the interface than if the SAM was protonated. As such, we could expect to see increases and decreases in the CH stretching modes associated with the alkane chain tilting back and forth minimizing electrostatic forces between the Au surface and the terminal end of the carboxylic acid SAM.

Finally, we will consider the positive going IR band at 1710 cm^{-1} which is associated with the protonated form of the carboxylic acid moiety [17, 18, 19, 20]. The analysis of this band is slightly complicated by the down going water band (1620 cm^{-1}). As this band is positive related to the reference potential spectrum (upward), we can conclude that we have a decrease in the protonated carboxylic acid moiety IR absorption of the MUA film at potentials negative the voltammetric peak.

Whether this is the result of the carboxylic acid becoming deprotonated with potential or the result of alkane chain tilting is difficult to ascertain at this point. For example, one would expect that if the MUA film has became deprotonated that we should see an increase in the carboxylate modes (~1450 cm^{-1}) [22, 23, 24] associated with a deprotonated film. This would show up in the spectrum as a negative going band. However, this feature is not present in the spectra in Figure 4.5 (or Figure 4.4 for that matter). As such, we can not conclusively state at this time which side of the peak is associated with protonated or deprotonated form of the carboxylic acid self-assembled monolayer.

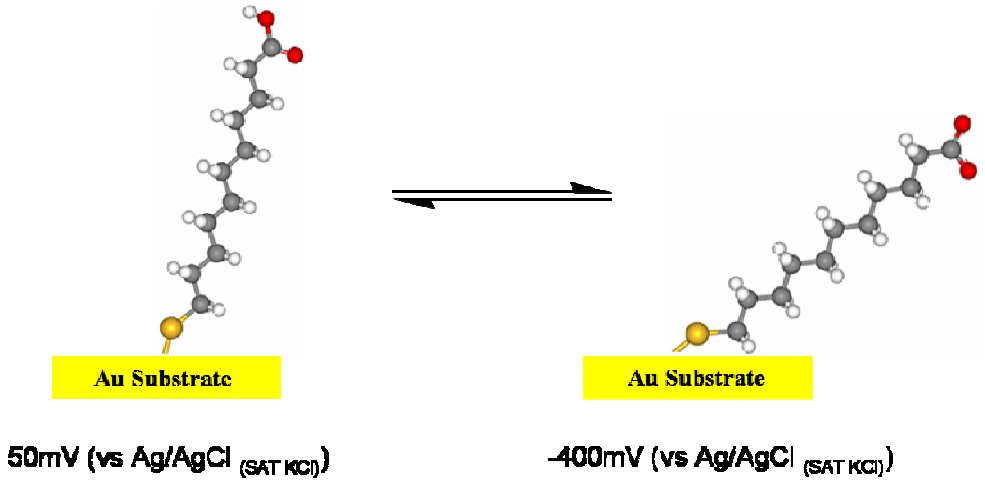

Figure 4.6. Tentative model of the protonation - deprotonation of MUA SAM as a function of potential.

However, there is some evidence that leads to a plausible model (Figure 4.6) for the electric-field driven protonation – deprotonation of MUA SAMs on gold substrates. From electrochemical measurements (Figure 4.3) we can see we have a

difference in the inner layer capacity at potentials on either side of the peak. This is consistent with a change in the dielectric constant for the SAM-electrolyte interface at potentials negative of the voltammetric peak. If we consider the SNIFTIR spectroscopic evidence, Figure 4.5, this tilt is also apparent by changes in the CH stretching modes around 2910 cm^{-1}. Accompanying this tilt is a loss of the IR signal related to the protonated carboxylic acid moiety (1710 cm^{-1}) suggesting that at potentials negative of the voltammetric peak associated with the electric-field driven protonation – deprotonation process our MUA SAM is deprotonated.

4.4 Conclusions

An inherit problem with *ex-situ* techniques is that in transferring the sample from an electrochemical environment the degree to which the interface is perturbed is difficult to quantify. The dramatic change of environment and the loss of potentiostatic control can give rise to uncertainties in the state of the film. As such an instrument was designed and implemented to allow us to measure electrochemical and spectroscopic information *in-situ.* Thus, we were able to ensure the electrode-electrolyte interface was maintained and to rule out any uncertainties associated with the *ex-situ* experiments.

At the onset we had difficulties incubating our Au plated Si ATR hemisphere using 4-MBA as the molecule of interest for our *in-situ* studies. The main cause of this was the Au thin layer would continually delaminate from the Si surface

preventing an *in-situ* experiment from working. Instead, we used SAMs incubated with MUA which had a much higher success rate than did 4-MBA when it came to incubating in the *in-situ* spectroelectrochemical cell. The decision to use MUA was because it shows very similar electrochemistry with the protonation-deprotonation reaction as 4-MBA.

After establishing what a protonated-deprotonated MUA film looks like by modifying the pH of the surrounding electrolyte, initial attempts to drive the protonation-deprotonation process electrochemically were performed. From these initial results we can not draw a concrete conclusion yet, but have formed a working hypothesis that could be further explored. What we have been able to determine is that the molecular structure at the surface does change as a function of applied potential, clearly evidenced by the reorientation of water molecules at the surface. Also, we have evidence indicating that the alkane chain backbone of MUA molecules tilt upon application of a potential resulting in changes in the CH stretching mode. We also have observed changes occurring in the carboxylic acid stretching modes with applied potential – whether it is from the backbone tilt, electric-driven deprotonation or a combination of the two, it is too early to draw any solid conclusions at this time. A more extensive study of this is beyond the scope of the current research, but does lay the ground work for further research opportunities.

4.5 References

[1] Erne, B.H.; Stchakovsky, M., Ozanan, F.; Chazalviel, J.-N., *J. Electrochem. Soc.* **1998**, *145*, 447.

[2] Tian, Z.Q.; Gao, J.S.; Li, X.Q.; Ren, B.; Huang, Q.J.; Cai, W.B.; Liu, F.M.; Mao, B.W., *J. Raman Spectrosc.* **1998**, *29*, 703.

[3] Chazalviel, J.-N.; Erne, B.H.; Maroun, F.; Ozanam, F., *J. Electroanal. Chem.* **2001**, *509*, 108.

[4] Iwasita, T. (Ed.), *Infrared Spectroscopy in Electrochemistry, Electrochim. Acta* **1996**, *41*, 621.

[5] Kunimatsu, K.; Uchida, H.; Osawa, M.; Watanabe, M., *J. Electroanal. Chem.* **2006**, *587*, 299.

[6] Osawa, M. in Alkire, R.C.; Kolb, D.M.; Lipkowski, J.; Ross, P.N. (Eds.), *Advances in Electrochemical Science and Engineering, Vol. 9*, Wiley-VCH Verlag GmbH & Co. KGaV, Chichester, UK, **2006**, pp. 269.

[7] Kaim, W.; Klein, A. (Eds.), Spectroelectrochemistry, Copyright 2008 Royal Society of Chemistry, Cambridge, UK.

[8] Yagi, I.; Nakabayashi, S.; Uosaki, K., *J. Phys. Chem. B* **1997**, *101*, 7414.

[9] Tadjeddine, A.; Peremans, A.; Guyot-Sionnest, P., *Surf. Sci.* **1995**, *335*, 210.

[10] Clarke, J.S.; Kuhn, A.T.; Orville-Thomas, W.J.; Stedman, M., *J Electroanal. Chem.* **1974**, *49*, 199.

[11] Zamlynny, V.; Lipkowski, J., *Advances in Electrochemical Science and Engineering* **2006**, *9*, 315.

[12] Grdadolnik, J., *Acta Chim. Slov.* **2002**, *49*, 631.

[13] Bewick, A.; Pons, S., in Clark, R.J.H., Hester, R.E. (Eds.), *Advances in Infrared and Raman Spectroscopy, Vol. 2*, Wiley-Heyden, Chichester, UK, **1985**, pp. 1.

[14] Miyake, H.; Ye, S.; Osawa, M., *Electrochem. Comm.* **2002**, *4*, 973.

[15] Delgado, J.M.; Orts, J.M., Perez, J.M.; Rodes, A., *J. Electroanal. Chem.* **2008**, *617*, 130.

[16] Burgess, I.; Seivewright, B.; Lennox, R.B., *Langmuir* **2006**, *22*, 4420.

[17] Nuzzo, R.G.; Dubois, L.H.; Allara, D.L., *J. Am. Chem. Soc.* **1990**, *112*, 558.

[18] Smith, E.L.; Alves, C.A.; Anderegg, J.W.; Porter, M.D., *Langmuir* **1992**, *8*, 2707.

[19] Arnold, R.; Azzam, W.; Terfort, A.; Wöll, C., *Langmuir* **2002**, *18*, 3980.

[20] Goutev, N.; Futamata, M., *Applied Spectroscopy* **2003**, *57*, 506.

[21] Ataka, K.; Yotsuyanagi, T.; Osawa, M., *J. Phys. Chem.* **1996**, *100*, 10664.

[22] Wells, M.; Dermody, D.L.; Yang, H.C.; Kim, T.; Crooks, R.M., *Langmuir* **1996**, *12*, 1989.

[23] Arnold, R.; Azzam, W.; Terfort, A.; Wöll, C., *Langmuir* **2002**, *18*, 3980.

[24] Zangmeister, C.D.; van Zee, R.D., *Langmuir* **2003**, *19*, 8065.

5 Conclusions

There is significant evidence from our electrochemical experiments to suggest that self-assembled monolayers of 4-mercaptobenzoic acid (4-MBA) can undergo protonation-deprotonation process by the application of an electric field. This is a comparable result to other carboxylic acid SAMs that have been studied for the same effect, particularly 11-mercaptoundecanoic acid (MUA). To further this evidence, means to examine the molecular structure of the surface were sought. This thesis describes successful application of External Reflectance Fourier Transform Infrared Spectroscopy (ER-FTIRS) and some initial attempts using i*n-situ* spectroelectrochemical techniques.

The electrochemical results measured for 4-MBA, show a voltammetric peak (not associated with the reductive desorption of the thiol) similar to SAMs of MUA that have been previously shown to be the protonation-deprotonation of the carboxylic head group [1]. We have also provided some IR spectroscopic evidence, showing the change in the state of the headgroup as a function of electric field potential and pH. This is evidenced by measurement of IR molecular vibrations

associated with carboxylic acid and the carboxylate moieties of the protonated and deprotonated forms of the carboxylic acid SAM respectfully.

Another phenomenon that was examined was the effect of various cations present in the electrolyte on the hydrogen bonding network formed by the carboxylic headgroups of the 4-MBA SAM. From these experiments, we noticed that divalent cations, particularly calcium, magnesium and barium, quench the protonation-deprotonation electric field driven reaction and is attributed to an exchange of the carboxylic acid protons with these cations. It should be noted that this effect was also present for monovalent electrolyte cations but the rate at which the exchange occurs is significantly slower.

Further experiments and literature [2, 3, 4, 5] looking at the hydrogen bonding network led us to add acetic acid to the incubation solution. By adding acetic acid to the ethanolic incubating solution the hydrogen bonding of neighbouring molecules on the surface is disrupted. To verify this fact we used External Reflectance FTIRS as the hydrogen bonding environment of the carboxylic acid moiety is very sensitive in the mid-IR region. From this data we were able to conclude that the lack of observed voltammetry with SAMs incubated in acetic acid is due to disruption of the hydrogen bonding network and subsequently the protonation-deprotonation reaction is quenched.

Initial studies of 4-MBA SAM for *in-situ* spectroelectrochemical measurements proved difficult and as such MUA was used as a substitute to try and provide some molecular level details of the protonation-deprotonation electric field driven reaction. The choice to use MUA was influenced by its long alkane backbone chain capable of forming tightly packed monolayers. These SAMs show similar electrochemical behaviour to 4-MBA SAMs. After designing and implementing the apparatus needed to make these measurements, techniques were developed to chemically plate Au onto the Si ATR element and software was written to acquire data and control the potential. Finally, a SAM of MUA was self-assembled onto the Au plated Si hemisphere prism from an ethanolic solution and then exposed to electrolytes of varying pH to get a global understanding of what the state of the SAM looks like protonated and deprotonated. Following this, an electric field was applied to the SAM toggling between two potentials to see the protonation and deprotonation of the SAM which was met with some success.

To summarize, the protonated state of SAMs of 4-MBA can be driven by the application of an electric field. This result is comparable to other carboxylic acid SAMs that have been studied so far. There are several factors that can quench this process, such as the nature of the hydrogen bonding network of the carboxylic acid moieties and the binding affinities of the electrolyte cations to the carboxylate moiety. *in-situ* spectroelectrochemical techniques should be able to provide a better description of what is happening at the interface.

5.1 Suggestions for Future Work

The vast majority of the work presented in the literature has a major focus on acid terminated SAMs, but there is no reason why base-terminated SAMs should differ in being able to potentially drive their protonation-deprotonation in an electric field. As such, it would be interesting to determine if there are any significant differences between the two. By continuing this line of research, one could effectively gain access to the appropriate conditions needed to electrically toggle various acid and base chemistries at the surface. Ultimately this would provide the framework to facilitate more complicated surface modifications for use as potential biosensors or biomimetic interfaces. For example, one could electrochemically direct the adsorption of particular analytes to our modified substrates for the use in disease detection applications.

With the initial successes of the electrochemical toggling experiments with the MUA SAMs using *in-situ* spectroelectrochemical techniques, one could foresee further studies of both MUA and 4-MBA SAMs (eventually extending into studies of base-terminated SAMs) to provide a more complete analysis of the surface. This could include answering some interesting questions about the kinetics of self adsorption for 4-MBA, MUA as well as base-terminated SAMs.

There was an initial report that also suggests that there is a ‘jamming effect’ of electrolyte ions occurring at the surface significantly slowing either protonation or

deprotonation of the acid moieties [6]. The authors measured the state of the COOH headgroup in a flow-through spectroelectrochemical cell by means of Second Harmonic Generation Spectroscopy. This technique is sensitive to changes in the dielectric values on the surface and can be used to infer the state of the COOH moiety. It would be very interesting to repeat a similar experiment except using a molecular structure sensitive technique, such as an *in-situ* ATR FTIR spectroelectrochemical technique, to further analyze this phenomenon.

Just to scratch the surface, one can see that there are still many interesting questions when it comes to fully understanding the electric-field driven protonation-deprotonation process of acid/base terminated SAMs and potential applications of these systems.

5.2 References

[1] Burgess, I.; Seivewright, B.; Lennox, R.B., *Lanmuir* **2006**, *22*, 4420-4428.

[2] Dannenberger, O.; Weiss, K.; Himmel, H.-J.; Jager, B.; Buck, M.; Woll, C., *Thin Solid Films* **1997**, *307*, 183.

[3] Arnold, R.; Azzam, W.; Terfort, A.; Woll, C., *Langmuir* **2002**, *18*, 3980.

[4] Willey, T.M.; Vance, A.L.; van Buuren, T.; Bostedt, C.; Nelson, A.J.; Terminello, L.J.; Fadley, C.S., *Langmuir* **2004**, *20*, 2746.

[5] Krause, P.F.; Katon, J.E.; Rogers, J.M.; Phillips, D.B., *Appl. Spectrosc.* **1977**, *31*, 110.

[6] Gibbs-Davis, J.M.; Kruk, J.J.; Konek, C.T.; Scheidt, K.A.; Geiger, F.M., *J. Am. Chem. Soc.* **2008**, *130*, 15444-15447.